國立交通大學

材料科學與工程研究所

碩士論文

應用鈀/鍺/銅歐姆接觸至全面銅金屬化之
磷化銦鎵/砷化鎵異質接面雙載子電晶體

Au-Free Fully Cu-Metallized InGaP/GaAs HBTs Using Pd/Ge/Cu Ohmic Contact to N-type GaAs

研 究 生：林家慶

指導教授：張 翼 博士

中 華 民 國 九 十 五 年 七 月

應用鈀/鍺/銅歐姆接觸至全面銅金屬化之磷化銦鎵/砷化鎵異質接面雙載子電晶體

Au-Free Fully Cu-Metallized InGaP/GaAs HBTs Using Pd/Ge/Cu Ohmic Contact to N-type GaAs

研 究 生：林家慶　　Student: Chia-Ching Lin

指導教授：張　翼 博士　　Advisor: Dr. Edward Yi Chang

國立交通大學

材料科學與工程研究所

碩士論文

A Thesis Submitted to Department of Materials Science and Engineering

College of Engineering

National Chiao Tung University

In Partial Fulfill of the Requirements

For the Degree of

Master of Science

In Material Science and Engineering

July 2006

Hsinchu, Taiwan, Republic of China

中華民國九十五年七月

應用鈀/鍺/銅歐姆接觸至全面銅金屬化之磷化銦鎵/砷化鎵異質接面雙載子電晶體

研究生:林家慶　　　　指導教授:張翼博士

國立交通大學材料科學與工程學研究所

摘要

在這篇論文中，成功的發展出使用鈀/鍺/銅歐姆接觸至N型砷化鎵上，且成功的運用至全面銅金屬化磷化銦鎵/砷化鎵異質接面雙載子電晶體中。

在低溫退火(250˚C)下，鈀/鍺/銅歐姆接觸即具備了低接觸電阻(5.73×10^{-7} Ω-cm^2)。經由X光繞射儀、穿透式電子顯微鏡、二次離子質譜儀和原子力顯微鏡的分析結果，鈀/鍺/銅歐姆接觸形成機制和微結構反應都已被研究了解；且鈀/鍺/銅歐姆接觸經過250˚C、24小時的熱穩定測試後，其接觸電阻幾乎沒有變化。

接著將鈀/鍺/銅歐姆接觸應用至全面銅金屬化磷化銦鎵/砷化鎵異質接面雙載子電晶體，並使用鉑/鈦/鉑/銅為P型砷化鎵歐姆接觸、鈦/鉑/銅為連接導線（其中鉑為銅之擴散阻障層)。量測結果顯示，全面銅金屬異質接面雙載子電晶體的直流特性和使用傳統金金屬化的特性相當；在微波特性方面，射極面積為3x20-μm^2之元件，其f_T為38GHz。此外，將元件施以

250°C、24 小時的熱處理後都很穩定，且在高電流密度 140kA/cm^{2}之電流加速測試 24 小時後，其元件特性也並沒有明顯改變。這些結果顯示將鈀/鍺/銅歐姆接觸應用至全面銅金屬化磷化銦鎵/砷化鎵異質接面雙載子電晶體其元件特性十分的優異。

Au-Free Fully Cu-Metallized InGaP/GaAs HBTs Using Pd/Ge/Cu Ohmic Contact to N-type GaAs

Student：Chia-Ching Lin **Advisor：Dr. Edward Y. Chang**

Department of Materials Science and Engineering

National Chiao Tung University

Abstract

In this study, a low contact resistivity Pd/Ge/Cu ohmic contact to n-type GaAs has been successfully developed. The Au-free fully Cu-metallized InGaP/GaAs HBTs using Pd/Ge/Cu ohmic contact to n-type GaAs also has been successfully fabricated for the first time.

The Pd (150 Å)/Ge (1500 Å)/Cu (1500 Å) ohmic contact exhibits a very low contact resistivity of 5.73×10^{-7} Ω-cm^2 at a low annealing temperature (250 °C). The ohmic contact formation mechanisms and microstructure evolution were investigated using x-ray diffraction (XRD), secondary ion mass spectrometry (SIMS), transmission electron microscopy (TEM), atomic force microscopy (AFM) and energy dispersive spectrometer (EDX). The thermal stability test of the Pd/Ge/Cu ohmic contact was also performed at 250 °C for 24 hours and showed no obvious degradation on Pd/Ge/Cu ohmic contact after the annealing.

The Pd/Ge/Cu ohmic contact was applied to fully Cu-metallized InGaP/GaAs HBTs. In this fully Cu-metallized HBT, Pt/Ti/Pt/Cu was used as the base metal, SiN_x was used for passivation, and Ti/Pt/Cu was used for interconnect metals with Pt as the diffusion barrier. The common emitter I-V

curves and Gummel plot of these Cu-metallized HBTs using Pd/Ge/Cu ohmic contact showed similar electrical characteristics as those for HBTs metallized with conventional Au-metallized HBTs. The cutoff frequency (f_T) of 3x20-μm^2-emitter-area devices was about 38GHz. During both the current-accelerated stress test (110 kA/cm^2 stress for 24h) and the thermal stability test (annealing at 250°C for 24 hours), for the fully Cu-metallized HBT with Pd/Ge/Cu ohmic contact showed almost no obvious degradation in electrical characteristics. The results show that the novel Pd/Ge/Cu ohmic contact can be used on Au-free fully Cu-metallized InGaP/GaAs HBTs, and exhibit good device performance.

誌　　謝

要感謝許多人的幫忙，才能使本論文能夠如期的完成。首先要感謝我的指導教授張翼博士，在我碩士班的研究生活當中，帶領我進入砷化鎵高頻元件的領域，提供完整的訓練及儀器資源。

其次我要感謝陳克弦學長、謝炎璋學長、李承士博士在實驗製程以及材料分析上提供寶貴的經驗以及建議，使我降低許多摸索的時間。還有要感謝國家奈米實驗室(NDL)及交大半導體中心，提供優良的儀器設備與環境，使實驗能夠順利進行。

另外我也要感謝連亦中學長、褚立新學長、黃瑞乾學長、張家源學長、許立翰學長、呂宗育學長、黃珍嬅同學、張家達同學、唐士軒學弟在實驗上的幫忙協助，以及詹前璋先生在儀器設備及廠務方面的幫忙，還有感謝莊蕙菁小姐在行政方面的協助幫忙。

最後，我要特別感謝我的父母親及又慈，感謝您們的關心、支持、包容與鼓勵，使我無後顧之憂，能夠專心順利完成學業，願這份榮耀與您們分享。

Contents

Abstract (in Chinese) I

Abstract (in English) III

Acknowledge (in Chinese) V

Contents VI

Table Captions VIII

Figure Captions IX

Chapter 1 Introduction 1

1.1 General Background 1

1.2 Outline of The Dissertation 2

Chapter 2 Literature Review 5

2.1 Ohmic Contact for GaAs-Based Devices 5

2.1.1 Requirements for A Good Ohmic Contact Material 5

2.1.2 Guideline for Low Resistance Ohmic Contact Formation 6

2.1.3 Ge-based Ohmic Contact Materials 8

2.2 GaAs Based Heterojunction Bipolar Transistors 11

Chapter 3 Experiment 25

3.1 Study of Ohmic Contact 25

3.2 Device Structure and Fabrication 26

3.2.1 Device Structure 26

3.2.2 Device Fabrication 27

Material Analysis and Electrical Characteristics Measurement 29
3.3 Specific Contact Resistance Measurement 29
3.4 Material Analysis of Ohmic Contact 30
3.4.1 X-ray Diffraction 30
3.4.2 Atomic Force Microscopy 31
3.4.3 Transmission Electron Microscopy 31
3.5 DC and RF Measurements 32
3.5.1 DC Measurements 32
3.5.2 RF Measurements 33
Chapter 4 Results and Discussion 39
4.1 Contact Resisitivity of The Pd/Ge/Cu Ohmic Contact 39
4.2 Formation Mechanism of The Pd/Ge/Cu Ohmic Contact 40
4.2.1 TEM and EDX for Microstructure Observation 41
4.2.2 X-ray Diffraction for Phase Identification 42
4.2.3 SIMS for Interfacial Elements Material Analysis 42
4.2.4 AFM for Surface Morphology Observation 43
4.3 Thermal Stability Test for The Pd/Ge/Cu Ohmic Contact 43
4.4 DC and RF Measurements 44
4.4.1 DC Measurements 44
4.4.2 RF Measurements 46
Chapter 5 Conclusions 69
Reference 71

Table Captions

Table 1 Properties comparisons of possible interlayer metals 4

Table 2 Summary of PdGe ohmic contact data from literature 14

Table 3 The typical epitaxial layer structure of the InGaP/GaAs HBT 34

Table 4 The lowest specific contact resistivities of Pd/GeCu ohmic contact on n-type GaAs with different Pd thicknesses. 47

Table 5 The lowest specific contact resistivities of Pd/Ge/Cu ohmic contact on n-type GaAs with different Ge thicknesses. 48

Figure Captions

Figure 1 Ideal interfacial structure for the low-resistance ohmic contact........... 15

Figure 2 Conduction mechanisms through metal/semiconductor interface with high donor doping level.. 16

Figure 3 Cross-section of the metal/semiconductor interface with ISL 17

Figure 4 The TEM image of the Pd /Ge contact after annealing at about 100℃ 18

Figure 5 (a) The structure and (b) TEM image of the PdGe contact 19

Figure 6 SIMS profiles of an Cu_3Ge contact formed at 400℃ for 30min.......... 20

Figure 7 TEM image of an Cu_3Ge contact formed at 400℃ for 30min 21

Figure 8 Schematic of the cross section of an HBT structure............................ 22

Figure 9 Energy band diagram of an HBT structure.. 23

Figure 10 The band diagrams of (a) a homojunction bipolar transistor and (b) a heterojunction bipolar transistor.. 24

Figure 11 Process flow of GaAs HBT 35

Figure 12 Illustration of transmission line methods (TLM) patterns.................. 38

Figure 13 Illustration of utilizing TLM identify ohmic contact resistance......... 38

Figure 14 The specific contact resistivity of the Pd(15nm) / Ge(150nm) / Cu(150nm) contact on n-type GaAs as a function of annealing temperature.. 49

Figure 15 The specific contact resistivity as a function of annealing temperature of Pd/Ge/Cu ohmic contact on n-type GaAs with different Pd thicknesses.. 50

Figure 16 The specific contact resistivities as a function of annealing

temperature of Pd/Ge/Cu ohmic contact on n-type GaAs with different Ge thickness. 51

Figure 17 The SEM image of the Pd(15nm) / Ge(150nm) / Cu(150nm) contact for the as-deposited sample. 52

Figure 18 (a) The TEM image of the Pd/Ge/Cu contact cross section, (b) The EDX profiles of the Ge/Cu compound grains after annealing at 150℃ for 20 min. 53

Figure 19 (a) The TEM image of the cross section of the Pd/Ge/Cu contact, (b) The EDX profile of the Cu_3Ge compound grains after annealing at 250℃ for 20 min. 54

Figure 20 (a) The TEM image of the cross section of Pd/Ge/Cu contact, (b) The high resolution TEM image of the interface between the metallic compound in the ohmic metal layer and the GaAs substrate after annealing at 250℃ for 20 min. 55

Figure 21 (a) The TEM image of the cross section of Pd/Ge/Cu contact, (b) The EDX profile of the near-interface region of the GaAs substrate after annealing at 250℃ for 20 min. 56

Figure 22 The TEM image of the cross section of the Pd/Ge/Cu contact after annealing at 400℃ for 20 min. 57

Figure 23 The X-ray diffraction patterns for the Pd (150 Å)/Ge (1500 Å)/Cu (1500 Å) contact after annealing at 250 °C for 20min, 400 °C for 20min, and the as-deposited sample. 58

Figure 24 SIMS profiles of the Pd (150 Å)/Ge (1500 Å)/Cu (1500 Å) contact after annealing at 250 °C for 20min. 59

Figure 25 The AFM images of (a) the Pd/Ge/Cu ohmic contact after annealing at 250℃ for 20 min, (b) the Au/Ge/Ni/Au ohmic contact after RTA at 380℃ for 30 sec. 60
Figure 26 The specific contact resistivities of the Pd/ Ge/ Cu ohmic contact and Au/Ge/Ni/Au ohmic contact on n-type GaAs as a function of aging time. 61
Figure 27 The OM images of Au-free fully-Cu InGaP/GaAs HBT with Pd/Ge/Cu as n-type ohmic contact device. 62
Figure 28 Comparison of the typical I_C-V_{CE} characteristics for the emitter area(4 x 20 μm^2) HBTs with Cu and with Au metallizations. 63
Figure 29 Comparison of Gummel plots for the emitter area(4 x 20μm^2) HBTs with Cu and with Au metallizations. 64
Figure 30 The current gain (β) as a function of stress time at constant I_B for the 4x20-μm^2-emitter-area fully Cu-metallized HBT with Pd/Ge/Cu ohmic contact... 65
Figure 31 Common emitter I-V curves measured before and after annealing at 250℃ for 24 h for the 4x20-μm^2-emitter-area fully Cu-metallized HBT with Pd/Ge/Cu ohmic contact. 66
Figure 32 The current gain (β) as a function of aging time at 250℃ for the 4x20-μm^2-emitter-area fully Cu-metallized HBT with Pd/Ge/Cu ohmic contact... 67
Figure 33 Current gain H_{21} curves measured for the 3x20-μm emitter-area fully Cu-metallized HBT.. 68

Chapter 1
Introduction

1.1 General Background

Copper metallization has been extensively used in the silicon industry since IBM announced its success in silicon very large scale integration process [1-3]. The advantages of copper metallization for Si technology include lower resistivity and higher electromigration resistance. A comparison of the characteristics of the metallization metals is list in Table 1. However, even though copper metallization has become very popular in the fabrication of Si devices, there are only a few reports on the copper metallization of GaAs devices [4-5]. Comparing to the commonly used Au metallization for GaAs industry, Cu has lower resistivity, higher thermal conductivity, higher electromigration resistance and lower cost. In our previous studies, backside copper metallization, Cu schottky structure in GaAs metal semiconductor field-effect transistors (MESFETs) [6], and the use of a copper air-bridge in low-noise GaAs high-electron-mobility transistors (HEMTs) [7], and the interconnect copper metallization using WN_X as the diffusion barrier in InGaP/GaAs heterojunction bipolar transistors (HBTs) has been reported previously[8].

The objective of this study is to develop the Cu-metallized ohmic contact for the GaAs devices to implement a fully copper metallized InGaP/GaAs HBTs. Conventionally, Au/Ge/Ni ohmic contact system is the most widely used material system for the n-type ohmic contacts of the GaAs-based devices.

However, this ohmic system was not compatible with other Cu metallization process. In addition, the Au/Ge/Ni ohmic contact system have several drawbacks, such as large spread of the contact resistivity, poor contact edge definition, and the annealing temperature was high due to the eutectic Au/Ge alloy (The Au-Ge eutectic temperature is 361 °C.).

This study reports a novel low resistance Pd/Ge/Cu ohmic contact system to n-type GaAs with a wide annealing temperature range (220 °C ~ 430 °C). A very low contact resistivity of 5.73 x 10^{-7} Ω-cm^2 was achieved at a low annealing temperature of 250 °C. In this study, the formation mechanisms of the Pd/Ge/Cu ohmic contact system will also be discussed.

Finally, the Pd/Ge/Cu ohmic contact was used for the emitter and collector metal of a fully Cu metallized InGaP/GaAs HBTs. The fully Cu-metallized used Pt/Ti/Pt/Cu for base metal, SiN for passivation, and Ti/Pt/Cu for interconnect with Pt as the diffusion barrier. The Cu-metallized base metal and interconnect metal used in this study which developed in our previous study [9]. The DC and RF characteristics of the fully Cu-metallized HBT are evaluated in this dissertation. Here, we are reporting for the first time the fabrication and electrical performance of the Au-free Cu metallized InGaP/GaAs HBTs with Pd/Ge/Cu as the emitter and collector ohmic contact metal.

Besides, the traditional GaAs HBTs using Au metallization as the ohmic and interconnect metal were also fabricated in order to compare the difference in device characteristics with the fully Cu-metallized GaAs HBTs.

1.2 Outline of The Dissertation

The contents of this dissertation include: literature review, experiment,

results, discussion and conclusions. In Chapter 2, the literature survey of ohmic contact for n-type GaAs and GaAs-based HBTs are reviewed. In Chapter 3, the study of ohmic contact, the samples preparation for material analysis, and the fully Cu-metallized GaAs HBT device process flow are described. Besides, the results of multilayer interfacial material analysis, the DC and RF device characteristics and the reliability tests for the fully Cu HBTs will also be presented. The Pd/Ge/Cu ohmic contact, formation mechanism, the DC and RF characteristics of the HBT devices using the Pd/Ge/Cu ohmic will be discussed in Chapter 4. Finally, the conclusions will be given in Chapter 5.

Table

Table 1 Properties comparisons of possible interlayer metals

Property	Cu	Ag	Au	Al
Resistivity(μΩ・cm)	1.67	1.59	2.35	2.66
Young's modulus · 10^{-11} dyn/cm^2	12.98	8.27	7.85	7.06
Thermal Conductivity (W/cm)	3.98	4.25	3.15	2.38
CTE · 10^{6}	17	19.1	14.2	23.5
Melting Point (℃)	1085	962	1064	660
Specific heat Capacity (J/Kg•K)	386	234	132	917
Corrosion in air	Poor	Poor	Excellent	Good
Deposion				
Sputtering	Yes	Yes	Yes	Yes
CVD	Yes	No	No	No
Evaporation	Yes	Yes	Yes	Yes
Etching				
Dry	No	No	No	Yes
Wet	Yes	Yes	Yes	Yes
Resistance to Electromigration	High	Very Low	Very High	Low
Delay Time(ps/mm)	2.3	2.2	3.2	3.7

Chapter 2
Literature Review

2.1 Ohmic Contact for GaAs-Based Devices

The definition of ohmic contact on a semiconductor is to allow electrical current to flow into or out of the semiconductor freely without barrier [10]. The contact should have a linear I-V characteristic, be stable over time and temperature, and contribute as little contact resistance as possible.

2.1.1 Requirements for A Good Ohmic Contact Material

The requirements for a good ohmic contact include: [11]

1. Low contact resistance

The first requirement for ohmic contacts of most devices is low contact resistivity, the resistance must be low enough not to affect the device I-V characteristics. The requirement for the reduction of the contact resistances has been continuing, because as the size of the device shrink to improve the device performance according to the scaling rule, the specific contact resistivity must decrease in order to keep the same contact resistance.

2. Thermally stable:

The second requirement for the ohmic contacts in GaAs devices is thermal stability during device fabrication and device operation.

In addition, a smooth surface, good adhesion, shallow horizontal and verticle diffusion depths, and low metal sheet resistance are required for ohmic contact in GaAs device. The requirements for ohmic contact are illustrated in

Figure 1.

2.1.2 Guideline for Low Resistance Ohmic Contact Formation

When a metal deposited on a semiconductor, the Fermi levels in the metal and the semiconductor must be equal. For the Fermi levels to be equal in both sides, an energy barrier $e\Phi_B$ must exist between the metal and semiconductor interface [12]. The carriers can not transport freely because of the energy barrier. The carrier transport mechanisms through the metal/semiconductor interface are strongly influenced by the doping concentration in the semiconductor and the temperature.

The current density (J) between contact metal and n-type semiconductor is shown below:

$$J = \exp(-q\Phi_B/E_{00}) \tag{2.1}$$

When

$$E_{00}=(qh/4\pi) \times (N_D/\varepsilon m^*)^{1/2}$$

ε :dielectric constant

N_D: doping concentration

m^*:effective electron mass

χ :electron affinity

Equation 2.1 indicates that the current density increases when the doping concentration increases. When the semiconductor is extremely heavily doped (>high-$10^{18}cm^{-3}$), the electrons can tunnel through the energy barrier between metal and semiconductor to form good ohmic contact. This is called "tunneling mechanism". The band diagram is shown in Figure 2.

Higher doping level is easy achievable in p-type GaAs. Because the dopants used in the p-type GaAs are not amphoteric and DX centers are associated with donors only, the ohmic contact to highly doped p-type GaAs can be easily formed. However, for n-type GaAs, the upper limit of the Si doping concentration achieved by the conventional ion-implantation technique is about 10^{18} cm^{-3}. This level is limited by the formation of DX centers in n-type GaAs.

Due to this limitation on the of doping concentration, the formation of ohmic contact on n-type GaAs is difficult. The best way to modify the interfacial microstructure to produce low resistance ohmic contact is to form a new intermediate semiconductor layer (ISL) with low energy barrier or high carrier density at the metal/semiconductor interface after heat-treatment as shown in Figure 3. This fabrication process are called "deposition and anneal ohmic contact" [11].

The most common method of forming "deposition and anneal ohmic contact" on n-type GaAs is to apply an appropriate metallization scheme to the heavily doped GaAs followed by annealing process. During the annealing process, one of the constituent metals diffuses into the wafer and dopes the cap GaAs layer heavily.

This ohmic contact fabrication technique needs a relatively simple fabrication system and with excellent reproducibility. Thus, this technique is suitable for manufacturing devices and used in a wide variety of GaAs devices.

However, the big disadvantage for this technique is that the process parameters can not easily be found, such as the contact metals, thickness of each metal layer, annealing time and temperature, diffusion coefficients, stress, surface energy, etc.

There are many kinds of "deposition and anneal ohmic contact" reported

from the literatures. Ge-based ohmic contact, one of the famous ohmic contact systems, will be described in the following section.

2.1.3 Ge-based Ohmic Contact Materials

AuGeNi contact materials were invented by Braslau et al. in 1967. [13], and have been extensively used as n-type ohmic contact materials for advanced GaAs devices over 30 years. Although AuGeNi ohmic contacts provided low contact resistance and excellent reproducibility, this ohmic contact also has several drawbacks such as rough surface morphology, deep reaction depth in GaAs substrate, complex alloying process, and thermal instability after contact formation. These reasons cause the large scale spread of the contact resistivity. To overcome these problems, many groups develop different ohmic contacts and try to apply them to the future sub-micron GaAs devices. The most popular ohmic contact system is Ge-based ohmic contact materials. Because Ge was found to dope heavily in the GaAs surface after heat-treatment, the contact resistivity of traditional Ge-based ohmic contacts is below $10^{-6}\Omega cm^2$ range.

In order to increase the donor concentration, a small amount of elements can be added. These additional elements increase the donor concentration in the GaAs surface layer and decrease the energy barrier height at the contact metal/GaAs interfaces.

To increase the donor concentration, “direct” doping elements and “indirect” doping elements were chosen in the past. The ”direct” doping elements were Sn, Sb, and Te which would increase the donor concentration in the GaAs surface layer by diffusing after heat-treatment. The “indirect” doping elements were Pd, Pt, and Au. Because the mixing enthalpy of the Ga with those elements (M) is smaller than that with As, Ga would form M-Ga phases with

these elements in the GaAs surface. And Ge atoms could easily diffuse to the Ga vacancies in the vicinity of the GaAs surface to increase the donor concentration in the GaAs surface layer and reduce the Rc values [14]. In addition, Ag and Cu also belong to the “indirect” doping elements with wide solubility with Ga in a wide temperature range, forming M(Ga) solid solutions [15]. The formation of M(Ga) solid solutions would also incease the Ga vacancy concentration and facilitate heavy doping of Ge atoms in the GaAs surface layer.

Pd/Ge/Cu ohmic contact is also one kind of the Ge-based ohmic contacts, but the formation mechanism is different from other Ge-based ohmic contacts reported in literature. Before introducing the formation mechanisms of Pd/Ge/Cu ohmic contact, PdGe and Cu_3Ge ohmic contact will be briefly introduced in next paragraphs.

Marshell et al. [16] developed the PdGe ohmic contact in 1980. PdGe ohmic contact is based on solid phase regrowth, not based on complex alloying process like traditional AuGeNi ohmic contact. The advantages of PdGe ohmic contact are uniform and shallow reaction, good thermal stability, and planer interface. The formation mechanism of PdGe is complex. When annealing at 100℃, Pd layer reacted with GaAs to form Pd_xGaAs ternary phase. The TEM image is shown in Figure 4 [17]. Because the mixing enthalpy of PdGa is smaller than PdAs, it could creat Ga vacancies in the near-interface region of the GaAs substrate. But at this temperature, ohmic contact is still not formed. After annealing above 300℃, the Pd reacted with amorphous Ge layer to form PdGe compounds and bring in some excess Ge atoms. Also at this temperature Pd_xGaAs ternary phase decomposed to form Pd atoms with GaAs layers. Then excess Ge atoms can dope the regrown GaAs layer and become highly doping

layer and finally excess Ge atoms become epitaxial crystal Ge layer between the regrown GaAs and PdGe layer. The final structure is shown in Figure 5. Table 2 shows the summery of the contact resistivity of PdGe contact from four literatures. The lowest contact resistivity was about 10^{-6} Ωcm^2 on n-type GaAs with Si doping concentration of 10^{18} cm^{-3}.

M. O. Aboelfotoh et al. [18] have developed the Cu_3Ge ohmic contact in 1994. This ohmic contact system is very unique. After annealing, Cu layer reacts with the Ge layer to become Cu_3Ge structure. Because the chemical potential of Ga atom in the Cu_3Ge is lower than that in the GaAs substrate, Ga atoms diffuse out to the Cu_3Ge compound and creat many Ga vacancies. Ge atoms can dope in near-interface region of GaAs to highly doping. It also can be seen by SIMS profile in Figure 6. Besides, this compound is crystal structure and has long range order. The grain boundary of Cu_3Ge compound is vertical to the GaAs surface. It can increase conductivity. The TEM image is shown in Figure 7.

Giving a summary of these two ohmic contact systems, the formation of the low resistance ohmic contact has two conditions. First, create Ga vacancies and then Ge atoms doping into near-interface region of GaAs substrate. It can use some elements reacted with GaAs to form ternary phase. And after annealing, MGaAs phase decomposed to metal and regrown n^+- GaAs layer same as the formation mechanism of the PdGe ohmic contact. It uses the chemical potential of Ga atoms in the ohmic compound is lower than in the GaAs so that Ga atoms diffuse out to create Ga vacancies as the formation mechanism of Cu_3Ge ohmic contact. Second, it forms the low resistivity metallic compound like Cu_3Ge crystal structure.

2.2 GaAs Based Heterojunction Bipolar Transistors

The concept of the heterojunction bipolar transistor was first introduced by William Shockley in 1948. A detailed theory related to this device was developed by H. Kroemer in 1957 [23]. Kroemer realized that the use of a wide-band-gap emitter and low-band-gap base would provide band offsets at the heterointerface that would favor the injection of the electrons, in an n-p-n transistor, into the base while retarding hole injection into the emitter. These advantages would be maintained, even when the base is heavily doped, as is required for low base resistance, and the emitter is lightly doped. Thus in an HBT, high emitter injection efficiency would be maintained while parasitic resistances and capacitances would be lower than for a conventional homojunction bipolar transistor.

The cross section of a basic n-p-n AlGaAs/GaAs heterojunction bipolar transistor is shown in Figure 8. The n-type emitter is formed in the wide-band-gap AlGaAs while the p-type base is formed in the lower band gap GaAs. The n-type collector, in this basic device, is also formed on GaAs. To facilitate the formation of the ohmic contacts, a heavily doped n^+-GaAs layer is present between the emitter contact and the AlGaAs layer. The energy band diagram of this device is shown in Figure 9.

Some inherent advantages of HBTs over silicon bipolar transistors are as follows [24]:

(1) Due to the wide-band-gap emitter, a much higher base doping concentration can be used, decreasing base resistance.

(2) Emitter doping can be lowered and minority carrier storage in the emitter can be made negligible, reducing base-emitter capacitance.

(3) High electron mobility, built-in drift fields, and velocity overshoot combine to reduce the electron transit time.

(4) Semi-insulating substrates help reduce pad parasitics and allow convenient integration of devices.

(5) Early voltages are higher and high injection effects are negligible due to high base doping.

Figure 10 shows the band diagram of a homojunction BJT and HBT. The energy band gap difference between the emitter and the base gives the HBT a substantial edge over BJT. When the base-emitter junction of a BJT is forward biased, both the electrons forward-injection into the base and the hole back-injected into the emitter experience the same amount of energy barrier. For the HBT, when the base-emitter junction is forward biased, the holes, which are back inject from the base into emitter, experience a $\triangle E_g$ larger energy barrier than the electrons, which are injected into the base. So, the HBT provides a design freedom meaning that a HBT structure design can have a heavily base dope to reduce the base resistance, while still maintaining a high current gain. We can quantify the advantage of HBT compared to BJT by calculating the ratio of the collector current to the base current [25].

$$\frac{Ic}{I} = \frac{D_{nB} X_E N_E}{D_{pE} X_B N_B} \frac{n_{iB}^2}{n_{iE}^2} = \frac{D_{nB} X_E N_E}{D_{pE} X_B N_B} \exp\left(\frac{\Delta E_g}{kT}\right) \tag{2.2}$$

Equation (2.1), which relates the intrinsic carrier concentration to the energy gap, was used in the derivation. It’s defined as the current gain which is one of the most important parameters in bipolar transistors.

Among several HBT device structures, InGaP/GaAs HBTs are becoming attractive as compared with the AlGaAs/GaAs HBTs in the circuit applications such as high-speed analog-to-digital converters, high-power microwave amplifiers, and high-speed optical communication circuits due to their robust reliability and excellent DC and RF performances. In addition, several advantages have been claimed for this material system, such as large valence-band discontinuity, very low interface recombination velocities with GaAs, significantly less oxidation in comparison with AlGaAs, no DX centers issue, and good selective etch with GaAs [26].

Table

Table 2 Summary of PdGe ohmic contact data from literature

Pd / Ge (Å)	ρ_c (Ωcm^2)	doping (cm^{-3})	Formation Condition	Ref.
500 / 1260	~10^{-6}	1×10^{18}	Anneal 325℃ for 30min	[18]
500 / 1260	2.84×10^{-6}	2×10^{18}	Anneal 330℃ for 30min	[19]
500 / 1250	1.4×10^{-6}	3×10^{18}	RTA 425 ℃ for 60sec	[20]
200 / 400	5.33×10^{-6}	2×10^{18}	RTA 350 ℃ for 45sec	[21]

1896

Figure

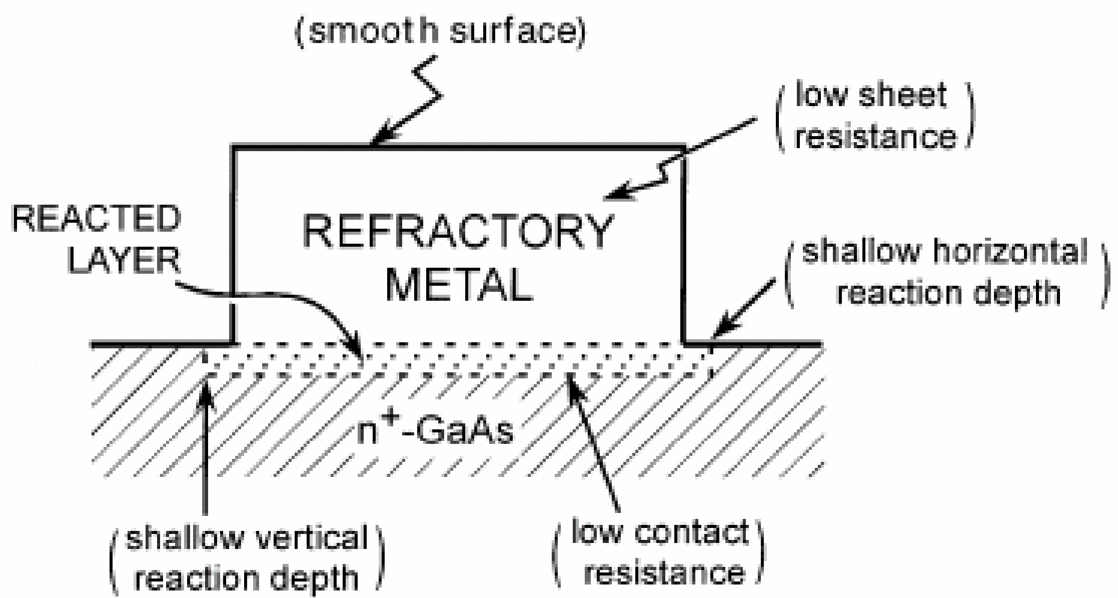

Figure 1 Ideal interfacial structure for the low-resistance ohmic contact

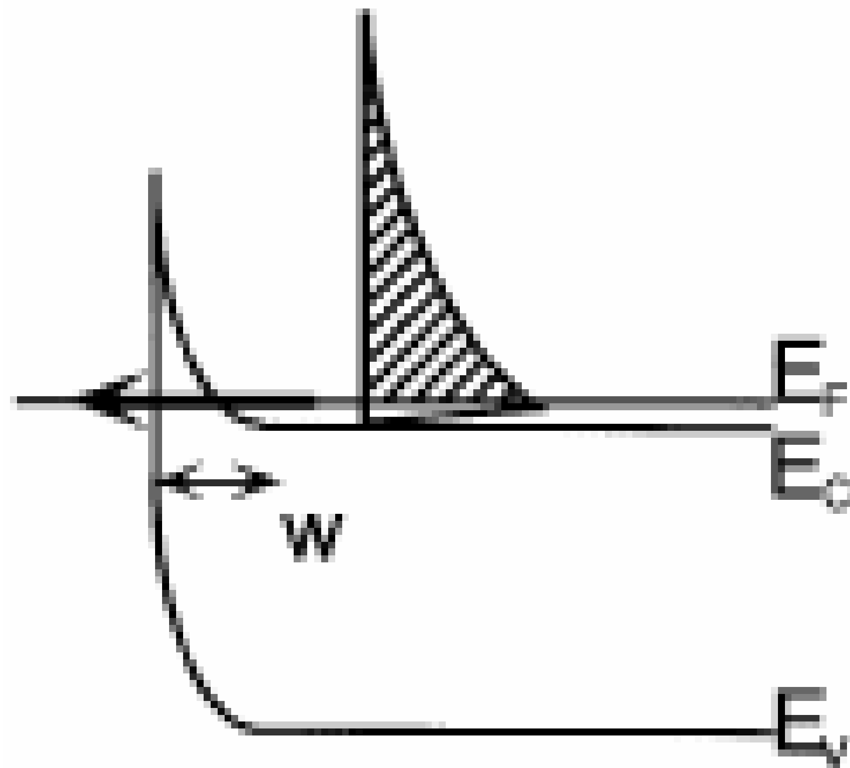

Figure 2 Conduction mechanisms through metal/semiconductor interface with high donor doping level

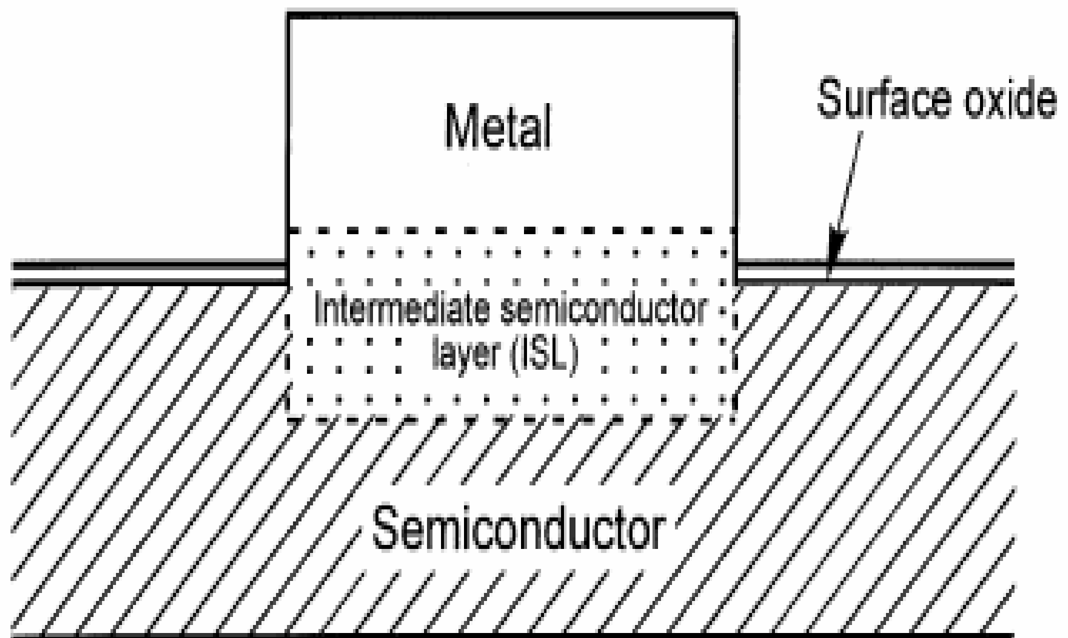

Figure 3 Cross-section of the metal/semiconductor interface with ISL

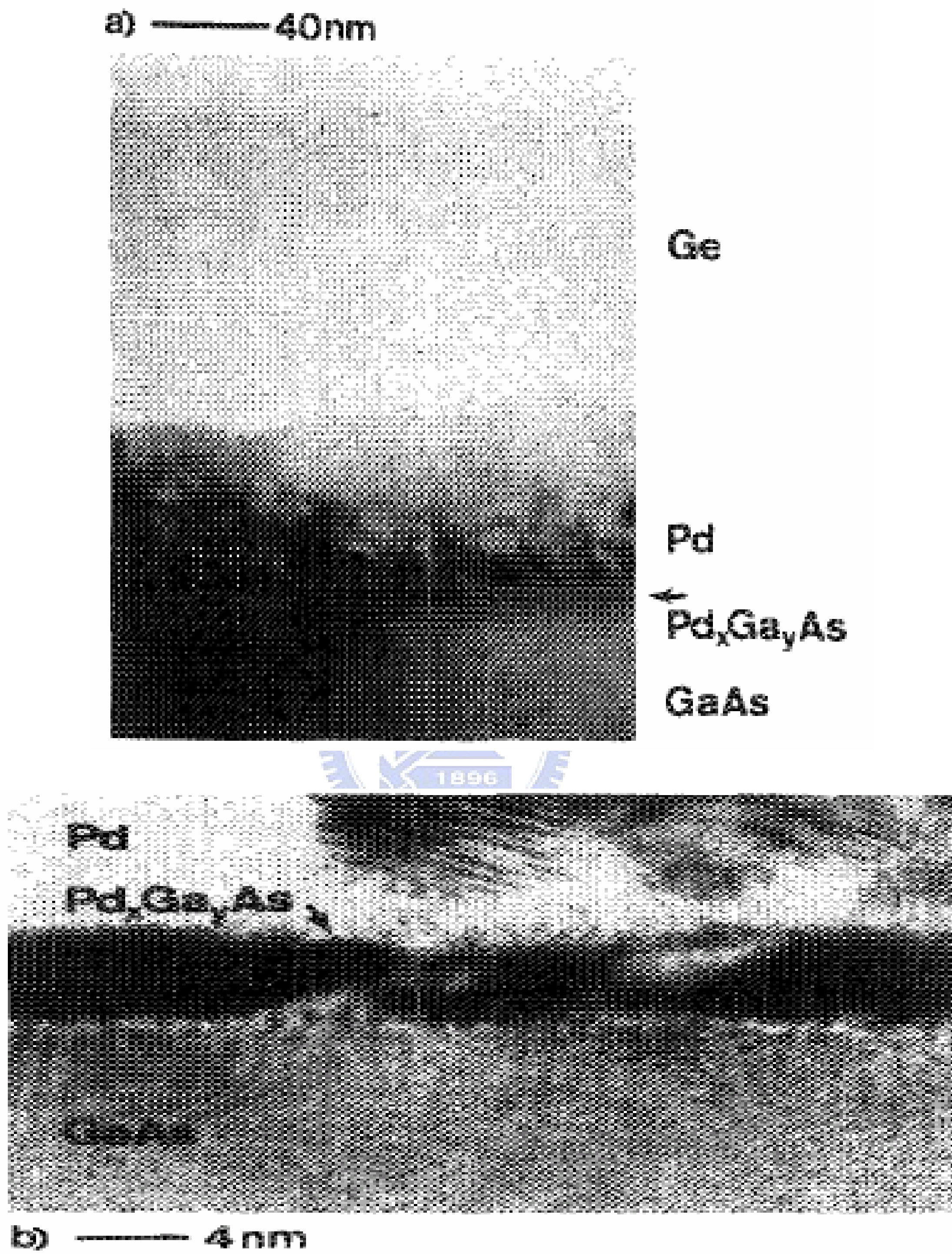

Figure 4 The TEM image of the Pd /Ge contact after annealing at about 100℃

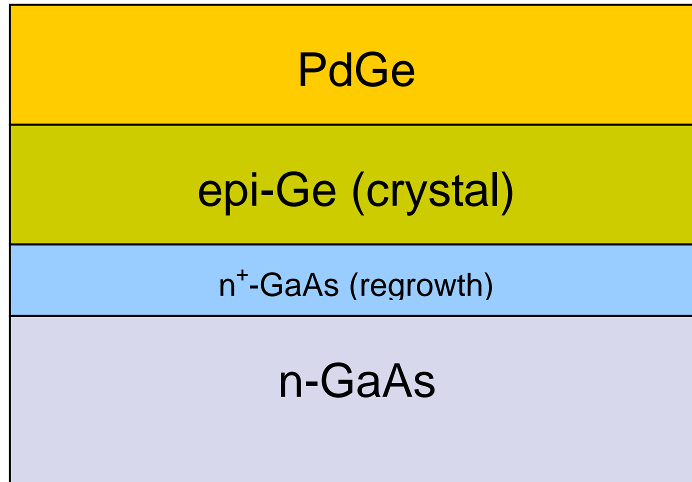

(a)

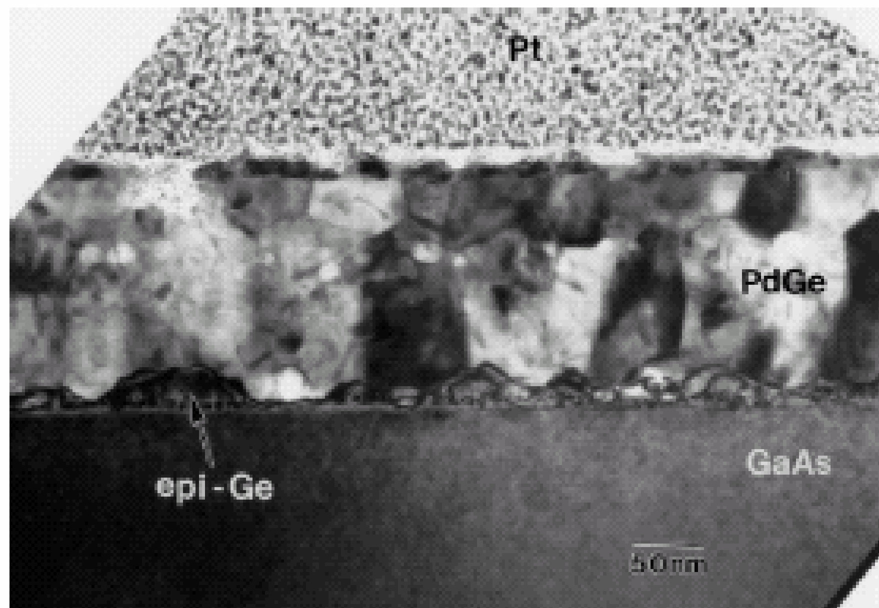

(a)

Figure 5 (a) The structure and (b) TEM image of the PdGe contact

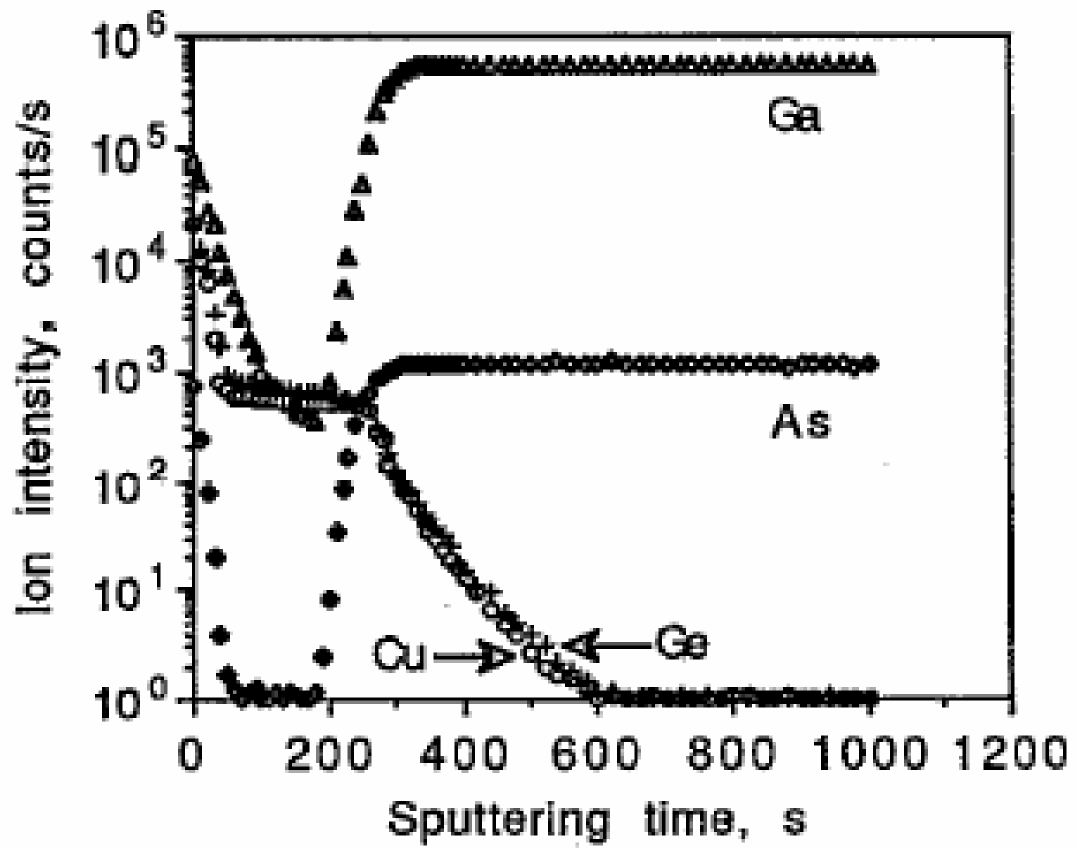

Figure 6 SIMS profiles of an Cu_3Ge contact formed at 400℃ for 30min

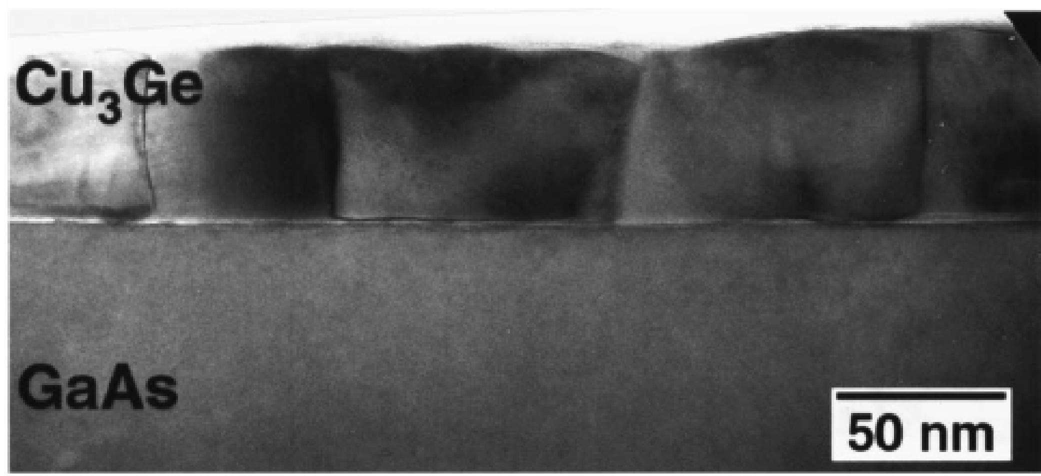

Figure 7 TEM image of an Cu_3Ge contact formed at 400℃ for 30min

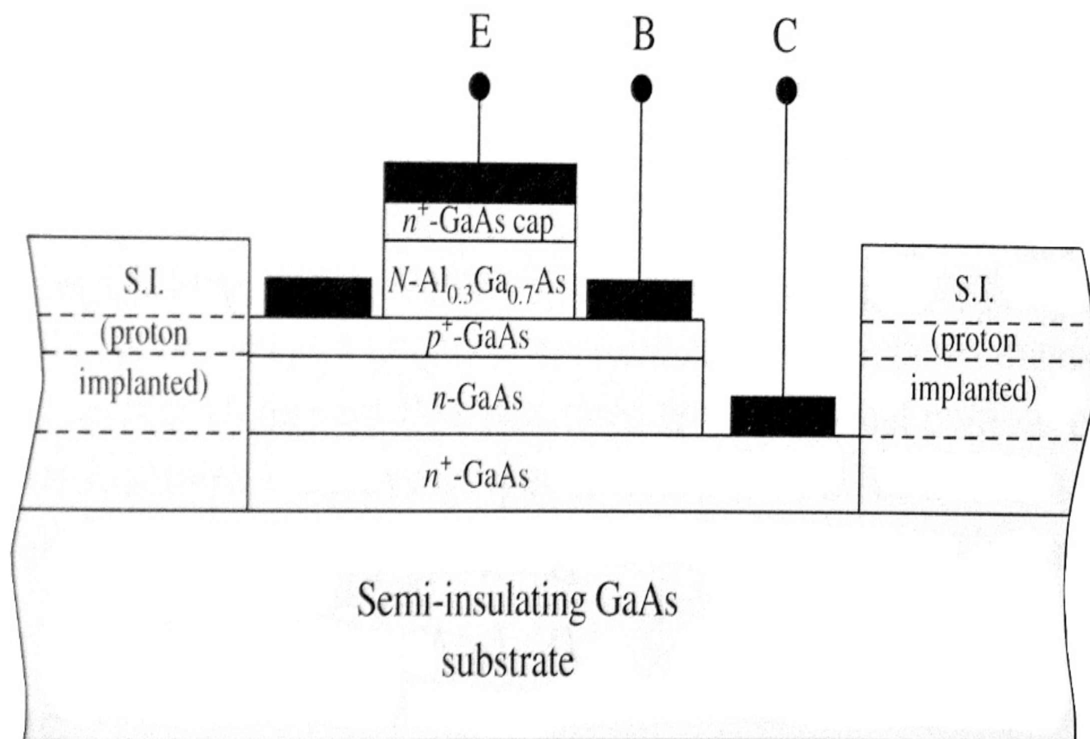

Figure 8 Schematic of the cross section of an HBT structure

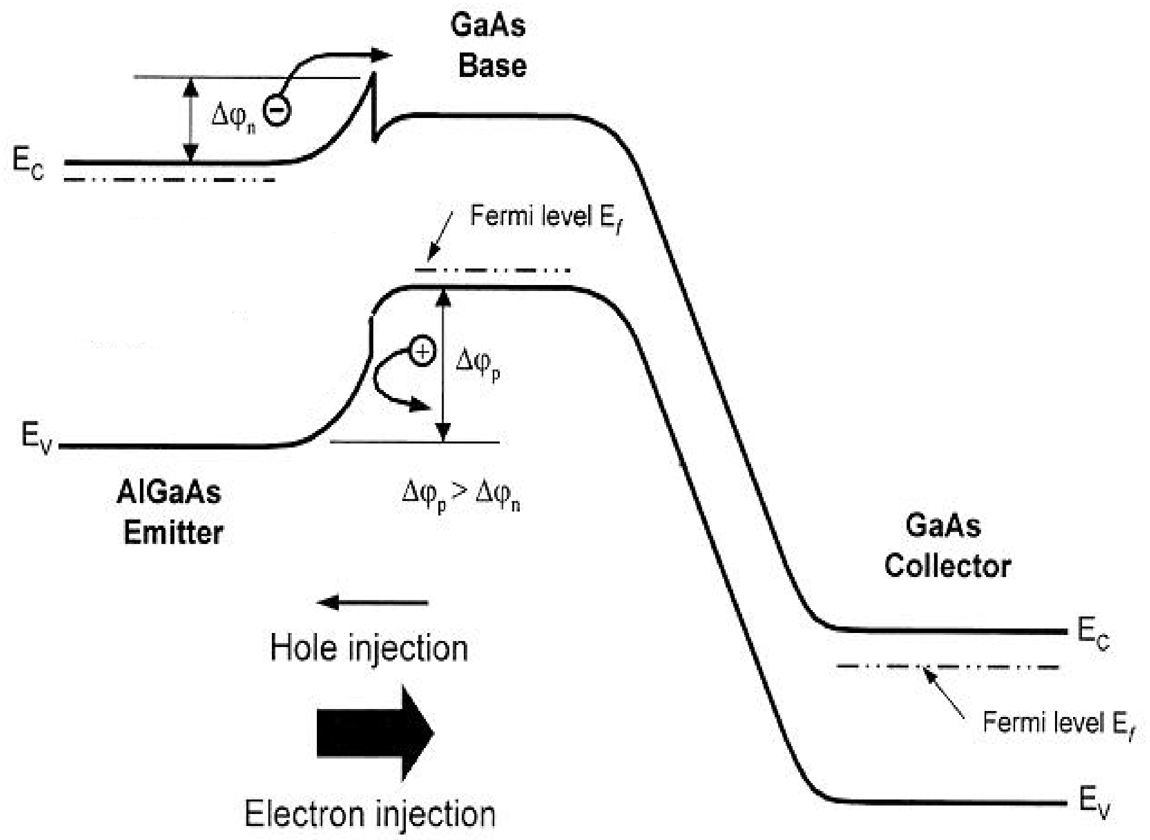

Figure 9 Energy band diagram of an HBT structure

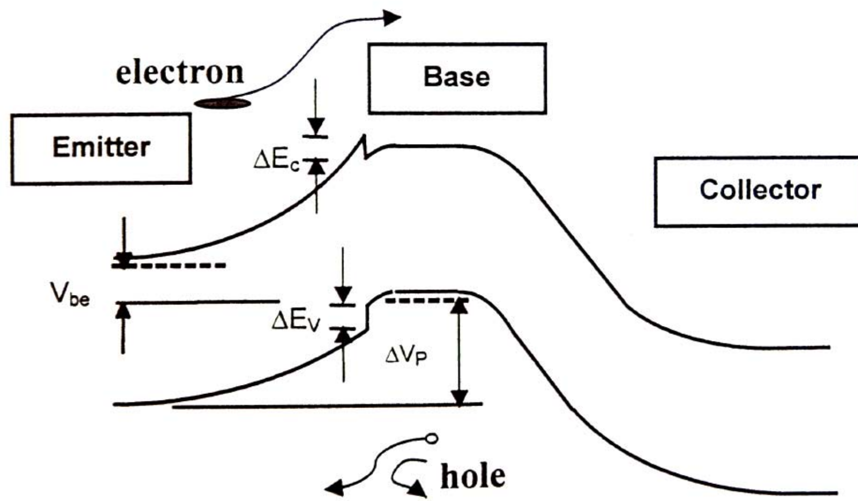

(a)

[watermark]

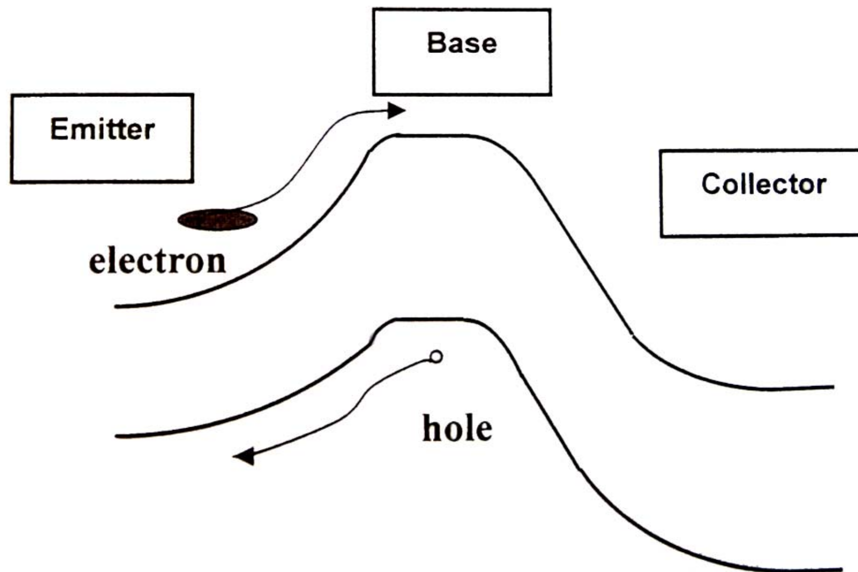

(b)

Figure 10 The band diagrams of (a) a homojunction bipolar transistor and (b) a heterojunction bipolar transistor.

Chapter 3
Experiment

The experiment can be divided into three parts. First, the Pd/Ge/Cu ohmic contact formation on n-type GaAs was studied. Second, the Pd/Ge/Cu ohmic contact was applied on the InGaP/GaAs HBTs as the n-type GaAs contact metal to form Au-free fully Cu-metallized InGaP/GaAs HBTs. Third, material analysis and electrical characterizations of the devices were performed.

3.1 Study of Ohmic Contact

The studies of ohmic contact include electrical characteristics measurement, material analysis, and thermal stability test.

The measurements of specific contact resistances of the n-GaAs/ Pd (15nm)/ Ge (150nm)/ Cu (150nm) were carried out by transmission line (TLM) method. The substrates used for the ohmic contact resistivity measurement in this study were semi-insulating GaAs wafers with Si-doped GaAs epitaxial layers (2000 Å, $1x10^{18}$ cm^{-3}). Standard photolithography was used to pattern the substrates for transmission line measurements (TLM). The GaAs mesa was etched by $H_3PO_4/H_2O_2/H_2O$ solutions. After the conventional organic solvent cleaning process, the substrates were chemically cleaned in a solution of HCl：H_2O (1：1 by volume) to remove the native surface oxide layer, the samples were load into the evaporation chamber. Pd (15nm)/ Ge (150nm)/ Cu (150nm) compositions were then deposited on the substrates using an electron-beam evaporator in a pressure of ~$1x10^{-6}$ Torr. The bulk of the resist and metal were

then removed by a wet solvent lift-off process, followed by a high pressure DI water rinse to remove the residues. After lift off, the samples were annealed in a conventional tube furnace at various temperatures from 150°C to 450°C in an N_2-ambient tube furnace for 20 minutes. The ohmic contact resistance (R_C) of the samples after annealing was measured using the transmission line model (TLM).

In order to understand the formation mechanism of Pd/Ge/Cu ohmic contact, the Pd/Ge/Cu multilayer was analyzed by XRD, TEM, SEM, and AFM. Phase identification was analyzed by the X-ray diffraction (XRD). The interface microstructure of the Pd/Ge/Cu ohmic contact materials/n-GaAs was observed by transmission electron microscopy (TEM) and scanning electron microscopy (SEM). The surface morphology was observed by atomic force microscope (AFM).

The thermal stability test of the Pd/Ge/Cu ohmic contact was performed by high-temperature annealing test (250°C) in a N_2-ambient tube furnace for 24 hours. The ohmic contact resistances (R_C) of the samples were measured using the transmission line model (TLM).

3.2 Device Structure and Fabrication

The epitaxial layers of the InGaP/GaAs single heterojunction bipolar transistors (SHBTs) were grown by molecular beam epitaxy (MOCVD) on semi-insulating (100) GaAs substrate.

3.2.1 Device Structure

The InGaP/GaAs HBT epitaxial layer structure is shown in Table 3.The

GaAs subcollector layer was grown on a 3-inch diameter semi-insulating substrate, and it was heavily doped to reduce the *n*-type ohmic contact resistance. The lightly *n*-type doped GaAs collector layer and the heavily *p*-type doped GaAs base layer were grown on it subsequently. The emitter layer is InGaP, and the heavily doped GaAs layer on the top serves as the ohmic cap layer.

3.2.2 Device Fabrication

The details of the Au-free fully Cu-metallized InGaP/GaAs HBT device fabrication are described as follows. Besides, the traditional Au-metallized InGaP/GaAs HBTs which use Au/Ge/Ni/Au and Pt/Ti/Pt/Au as *n*-type and *p*-type ohmic contacts metals and Ti/Au as the interconnect metal were also fabricated for comparison. The flow charts of the process flow for device fabrication were shown in Figure 11.

The first step is wafer clean. The wafers were immersed into ACE and IPA separately, each for five minutes to remove any contaminants from the wafer surface, and then they were blown to dry by nitrogen gas.

The second step is emitter mesa, collector mesa, and isolation etching. The InGaP/GaAs HBT devices were fabricated using a standard triple mesa process. The GaAs layers were etched by etchant composed of phosphoric acid, hydrogen peroxide, and D.I. water. And the InGaP layer was etched by a mixture of phosphoric acid and hydrogen chloride acid. After each etching process, the devices were rinsed by D.I. water and blown dry by nitrogen gas. The first step of the fabrication was to define the emitter mesa area. The emitter mesa was etched and stopped on the InGaP emitter layer. The collector mesa was etched and stopped on the GaAs subcollector layer. During the isolation etch, the GaAs subcollector was etched to the extent of undercut to separate each devices and to

reduce the leakage current from the substrate. The process flow diagrams of the triple mesa process are shown in Figure 11.1-Figure 11.3.

The third step is the emitter and collector metal deposition. The metallization metals in this fabrication were all defined by AZ5214E photo resist. After the metallization, a standard lift off process was used to remove the unwanted metals. The emitter and collector ohmic contacts were Pd (15 nm)/Ge (150 nm)/Cu (150 nm). After the emitter and collector metal depositions, a high temperature alloying process using tube furnace was conducted to form the ohmic contacts. To confirm the alloying process, the ohmic contact resistance of device was measured in process control monitor by using the transmission line model (TLM) method. The diagram of the metal deposition process is shown in Figure 11.4.

The fourth step is base metal deposition. For GaAs HBTs, the base layer is formed by GaAs with carbon doping to form p^+ type doping. In order to form ohmic contact on p^+-GaAs layer, the Pt (5 nm)/Ti (20 nm)/Pt (60 nm)/Cu (100 nm) was used. Before the deposition of the base metal, the material of GaAs emitter layer under the base ohmic contact photo-resist opening was etched to expose the underlying base layer. The metals were all deposited by e-gun evaporator and completed by lift off process. The diagram of the process flow of the base metal deposition is shown in Figure 11.5

The final step is passivation, contact via etching, and metal line deposition. Device passivation was realized by 100 nm PECVD silicon nitride film. This passivation protects the critical area of the originally exposed wafer surface from humidity, chemicals, gases, and particles. Passivation Vias between ohmic contact metals and interconnect metals were etched by reactive ionic etcher (RIE). The schematics of the device passivation and contact via are as shown in

Figure 11.6-Figure 11.7. After opening the connecting via on the nitride film, the Ti (30 nm)/Pt (60 nm) and interconnect Cu (400 nm) metals were sequentially deposited by e-gun evaporator over patterned resist. The metals were then removed by an ACE wet solvent lift-off process, followed by a high pressure DI water rinse to remove the residues. The schematic of the finished device is as shown in Figure 11.8. After all process, the DC and RF characteristics of the HBT devices were measured using an HP4142B and HP8510C network analyzer. The devices were stressed using a high-temperature thermal annealing test and a current-accelerated test for reliability evaluation.

Material Analysis and Electrical Characteristics Measurement

3.3 Specific Contact Resistance Measurement

The specific resistance was measured by KEITHLEY 2400 SourceMeter using TLM method.

The transmission line method (TLM) pattern, as illustrated in Figure 12, was designed in the process control monitor (PCM) in order to measure the ohmic resistance and to identify the ohmic contact characteristics. The resistance between two adjacent electrodes is expressed by the following equation

$$R = 2R_C + R_S L/W \quad (3.1)$$

where R is measured resistance, R_C is contact resistance, R_S is sheet resistance of channel region, W is electrode width, and L is the space between electrodes.

The resistance between the two adjacent electrodes can be plotted as a function of the space between electrodes. In this study, the distances between TLM electrodes are, 2.5 um, 3.5 um, 4.5 um, and 6.5 um, respectively. The plot

is shown in the Figure 13. Extrapolating the data to L=0, one can calculate a value for the term R_C. The specific contact resistance ρ_C is defined by

$$\rho_C = \frac{W^2 R^2}{R_S} \tag{3.2}$$

3.4 Material Analysis of Ohmic Contact

The formation mechanism of the Pd/Ge/Cu ohmic metal was analyzed by XRD, AFM, and TEM. These methods are briefly introduced as follow.

3.4.1 X-ray Diffraction

The phase transformation of the samples annealed at different temperatures was identified by Bede D1 High Resolution X-ray diffractometer.

X-rays are not readily reflected by crystal surfaces like a mirror, rather they are scattered through many atomic layers. *X*-rays can however appear to be reflected by ordered layers of atoms or molecules if the distance between the layers, as seen from the oblique viewpoint of an incoming *X*-ray, is the same as the X-ray wavelength. The scattered *X*-rays from each layer reinforce in the direction of a detector positioned as though it was going to collect a reflected signal. Knowing the combined angle of tilt (2theta) of the *X*-ray source and the detector relative to the sample surface, the spacing between the atomic layers can be calculated, as long as the *X*-ray wavelength is known. This is the *d* spacing. It is directly related to the sine of the tilt angle.

There are infinite sets of d spacings in a crystalline solid. Crystals typically have many different atomic layers in different directions. Atoms or molecules occupying layers in some directions are densely packed with atoms (scattering centers). Stronger signals are observed than with less densely packed layers in

other directions. A scan from 10 degrees to 90 degrees usually yields a diffraction pattern unique to that crystal.

The operation voltage of the XRD used in our study is 40 kV and the operation current is 30 mA. The X-ray is from the K_{α} peak of Cu (K_{α}=1.5406$\mathring{A}$) which is filtered by Ni-filter. The angle between the X-ray and the sample was θ= 5~45 degree. The detector scanned the samples between 2θ= 10~90 degrees. The θ and 2θ angle is conformed to Bragg's Law.

3.4.2 Atomic Force Microscopy

The surface morphology was observed by using atomic force microscopy (AFM).

The AFM is commonly employed to detect changes in surface structure on the atomic scale. The AFM has a cantilever which has a sharp, force-sensing tip at its end. It is the tip that interacts with the surface of the sample. As the interaction force between the cantilever tip and the surface varies, deflections are produced in the cantilever. These deflections may be measured, and used to compile a topographic image of the surface. In our experiment, we use Digital Instrument AFM (MultiMode) for surface morphology observation.

3.4.3 Transmission Electron Microscopy

Knoll and Ruska (1932) developed the idea of electron lenses and Ruska received Nobel Prize in 1986. The transmission electron microscopy is analytical tool that allows detailed micro-structural examination through high-resolution and high-magnification imaging. It also enables the investigation of crystal structures, orientations and chemical compositions in phases,

precipitates and contaminants through diffraction pattern, x-ray, and electron-energy analysis. In our experiment, we use JEOL HRTEM (JEM-2100F) for microstructure observation and EDX analysis. It can achieve magnifications of up to 800,000X and detail resolution below 1 nm. Quantitative and qualitative elemental analysis can be provided from features smaller than 2nm. TEM is one of the most powerful tool for material analysis. But sample preparing is always a difficult and time consuming process. Since the electron beam must trans-through the specimen and remain bright enough to get image, the specimen must be thinned to less than 100nm, and even less than 50nm for high resolution. The common way of specimen and the other is heating. So we must take care in all steps.

3.5 DC and RF Measurements

3.5.1 DC Measurements

The DC current-voltage (*I-V*) characteristics of the HBT devices were measured by HP4142B. The collector to emitter voltage (V_{CE}) was biased from 0 to 3 volts for the 3×20 um^2 and 4×20 um^2 emitter area HBT devices. During the measurement of the *I-V* curves, there were three probes contacted onto the pads of emitter, base and collector.

In this study, the DC characteristics (common emitter I-V curve and gummel plot) of the Cu-metallized InGaP/GaAs HBT with Pd/Ge/Cu ohmic contact were compared with the traditional Au-metallized HBT.

Au-free fully Cu-metallized InGaP/GaAs HBT with Pd/Ge/Cu ohmic contact were tested by using current accelerated test and high-temperature thermal annealing test for reliability evaluation. The high current test was

performed at a high emitter current density of 110kA/cm^2 at collector-emitter voltage of 1.5V for 24 hours. The thermal annealing test was carried out by annealing at 250℃ for 24 hours in nitrogen ambient.

3.5.2 RF Measurements

The RF performance of the HBT devices was characterized by on-wafer-*S*-parameter measurements using HP8510C network analyzer before and after the thermal annealing test. The *S*-parameters were measured in frequencies ranging from 1 to 40 GHz. Cutoff frequency (f_T) and maximum frequency of oscillation (f_{max}) are often used to characterize the devices. These two quantities represent the unity gain intercept point of the short circuit current gain (h_{21}) and the unilateral power gain (U). Each parameter can be computed from *S*-parameter data.

The h_{21} as a function of frequency were measured under collector-emitter voltage (V_{CE}) of 2V, 2.5V, and 3V. The base current was 0.06, 0.08, 0.1, 0.12, 0.14mA. The f_T was extrapolated with -20 dB/decade slope.

Table

Table 3 The typical epitaxial layer structure of the InGaP/GaAs HBT

Layer	**Material**	**Type**	**Doping**	**Thickness（Å）**
Emitter Cap	GaAs	*n*+	5×10^{18}	2000
Emitter	InGaP	*n*	3×10^{17}	500
Base	GaAs	*p*+	4×10^{19}	800
Collector	GaAs s	*n*-	2×10^{16}	7000
Subcollector	GaAs	*n*+	5×10^{18}	5000
Substrate	GaAs			

Figure

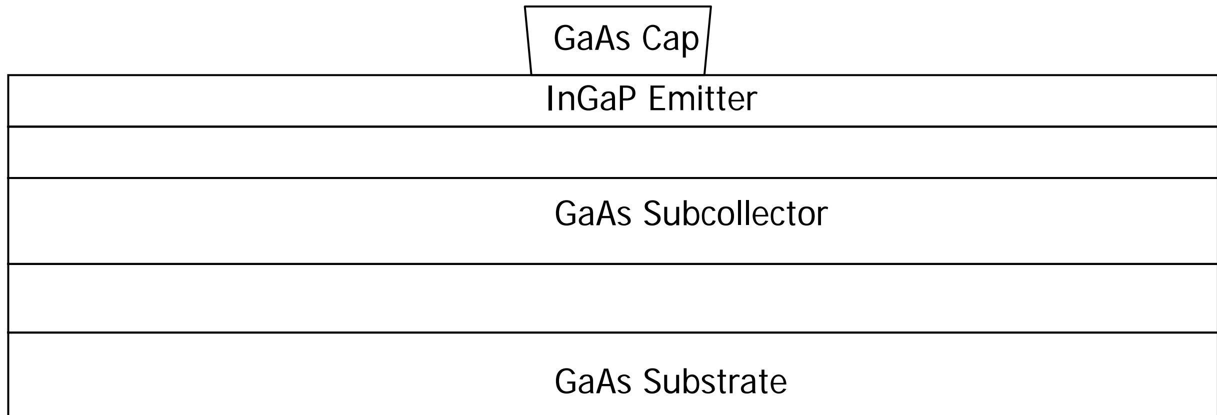

Figure 11.1 Emitter mesa etch

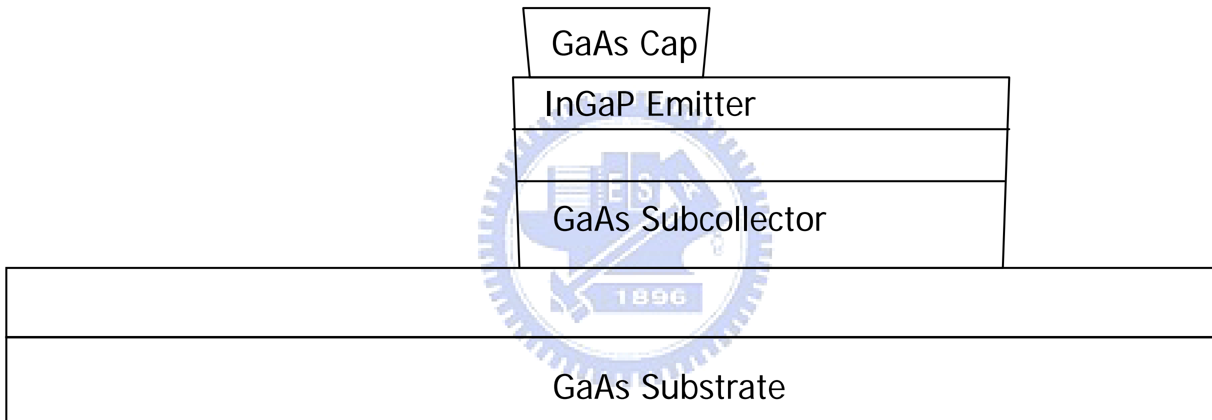

Figure 11.2 Base and collector mesa etch

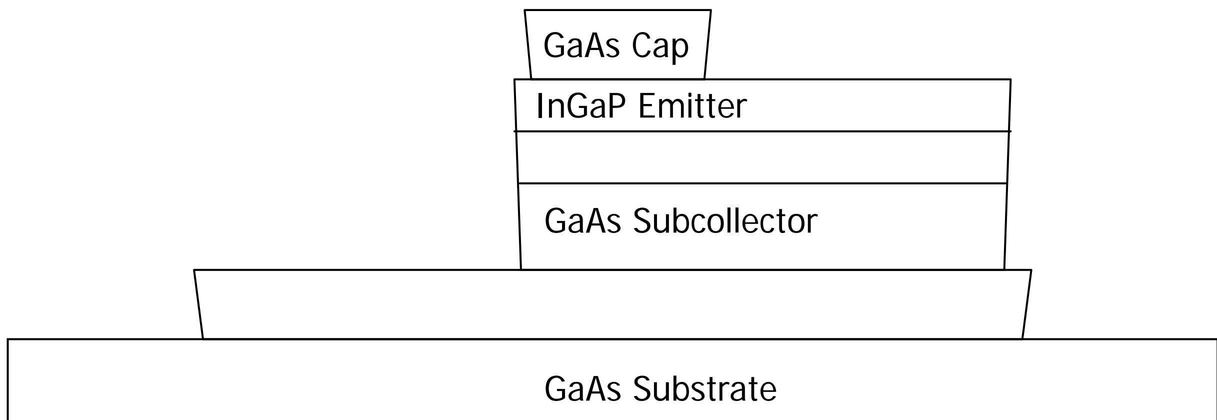

Figure 11.3 Mesa isolation

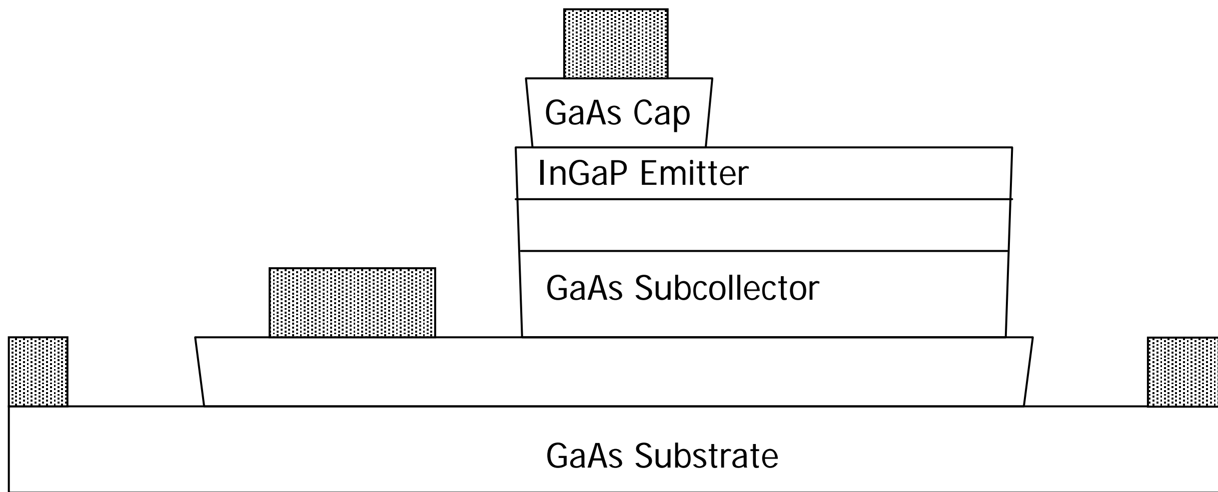

Figure 11.4 Emitter and collector ohmic contact metal formation

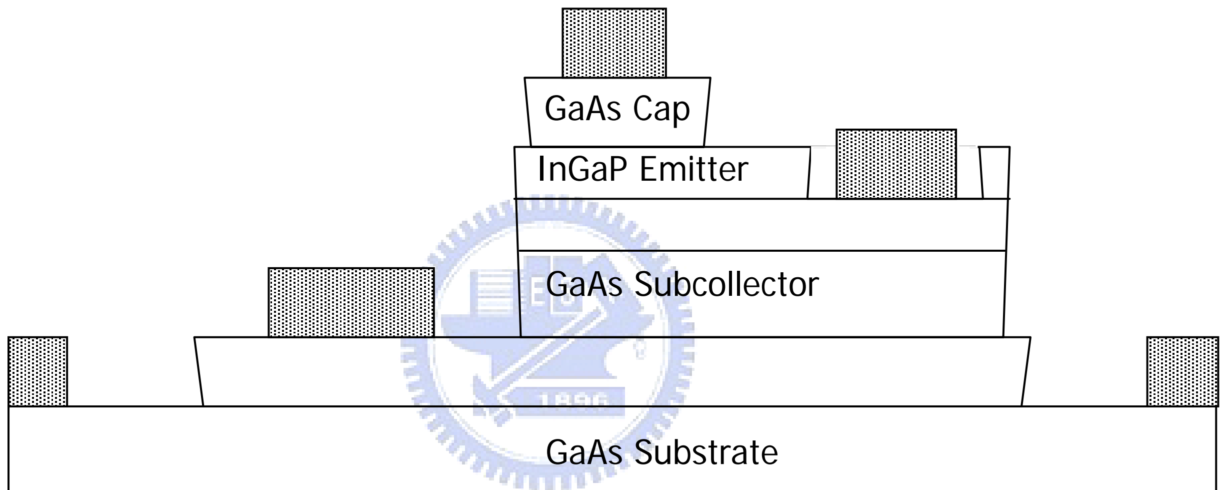

Figure 11.5 Base ohmic contact metal formation

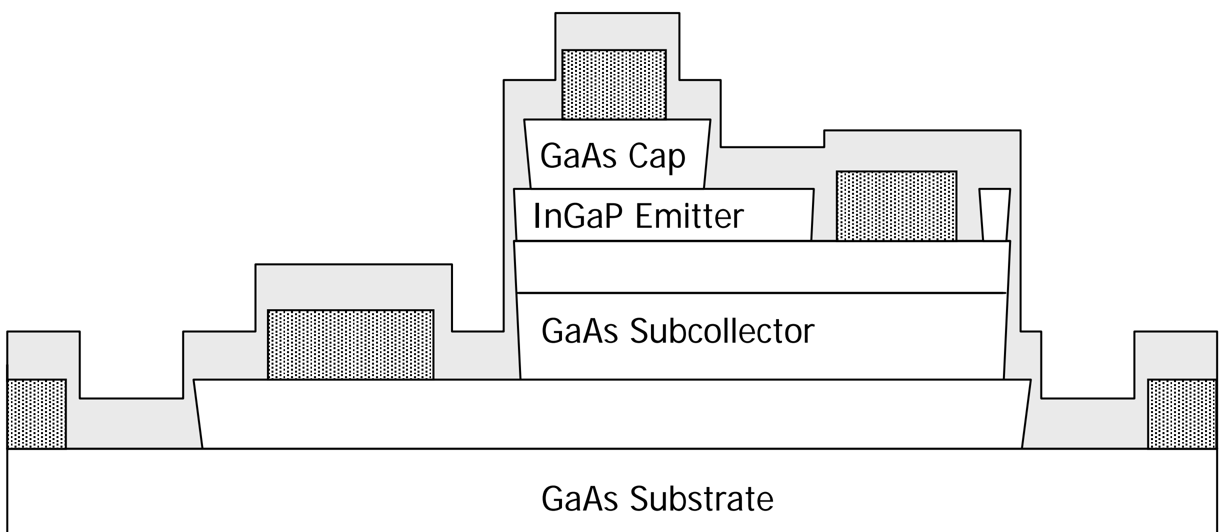

Figure 11.6 Silicon Nitride Deposition

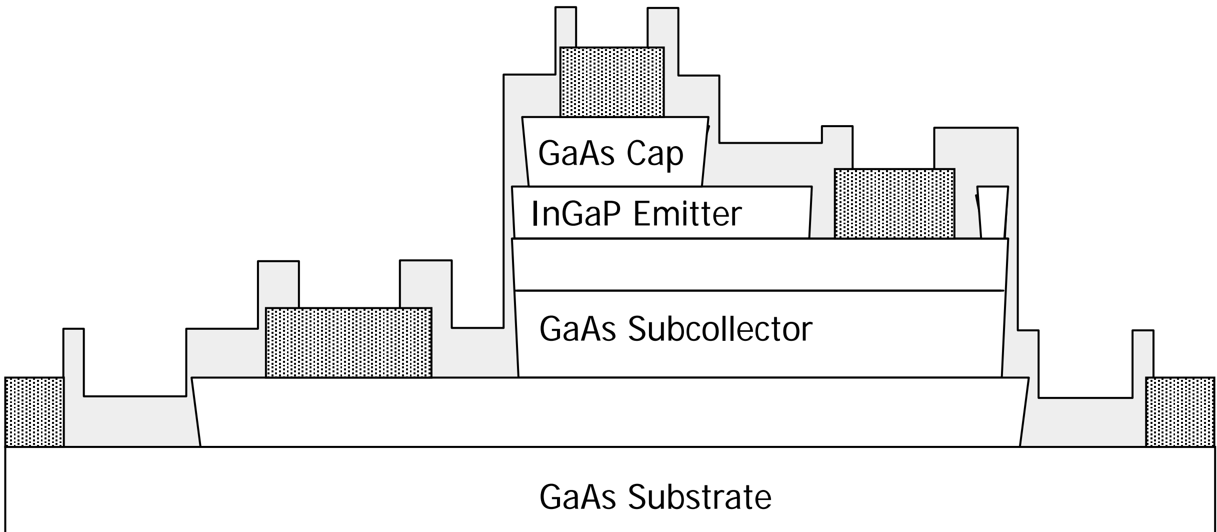

Figure 11.7 Nitride via etch

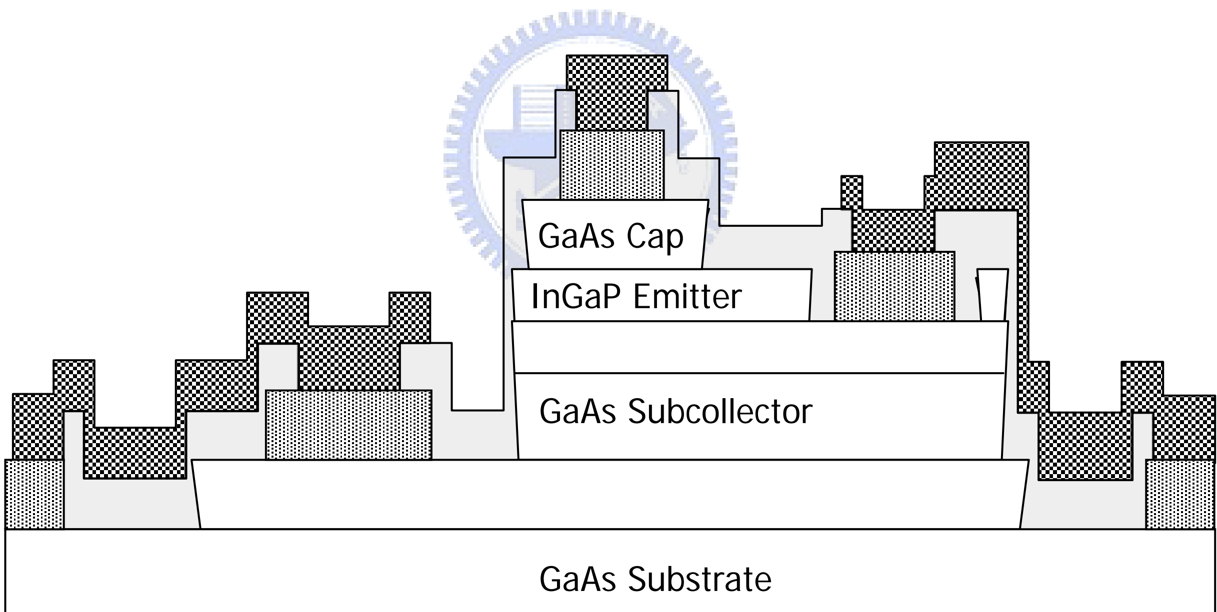

Figure 11.8 Interconnect metal line

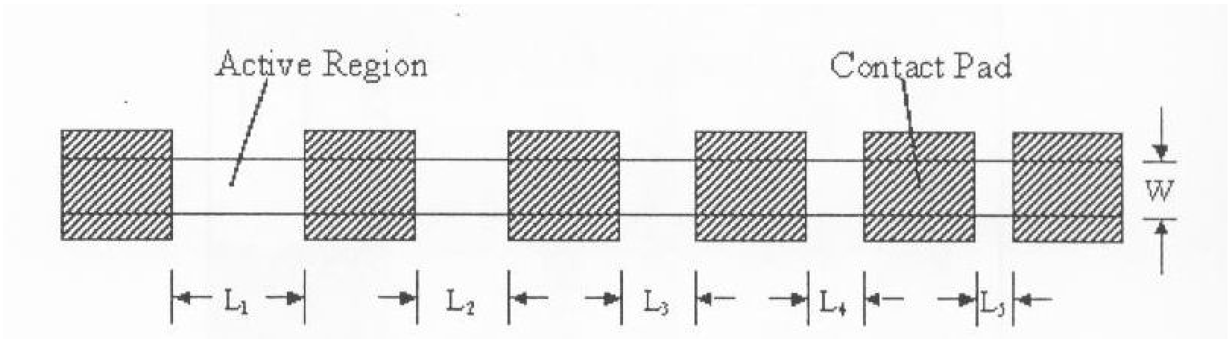

Figure 12 Illustration of transmission line methods (TLM) patterns

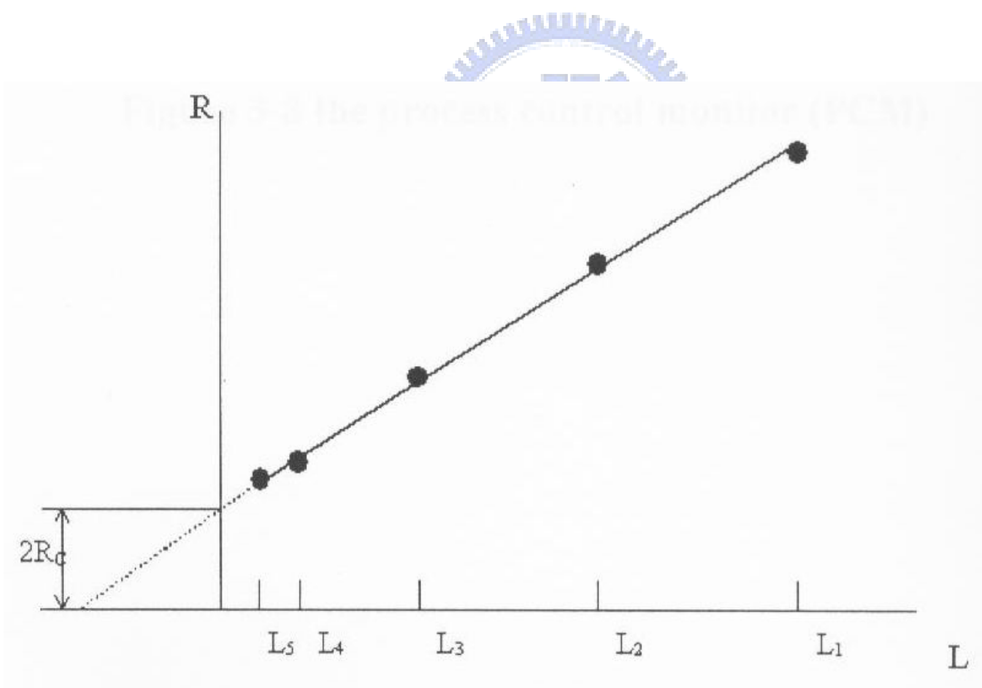

Figure 13 Illustration of utilizing TLM identify ohmic contact resistance

Chapter 4
Results and Discussion

In this chapter, the contact resistivity and the thermal stability of Pd (150 Å)/Ge (1500 Å)/Cu (1500 Å) ohmic contact on n-type GaAs are shown. After that, the formation mechanism of the Pd/Ge/Cu ohmic contact was investigated using the results of XRD, SMIS, AFM, TEM and EDX. In the last half of the chapter, the results of DC and RF measurements of Au free fully Cu-metallized InGaP/GaAs HBT using Pd/Ge/Cu ohmic contact are shown.

4.1 Contact Resisitivity of The Pd/Ge/Cu Ohmic Contact

The Pd (150 Å)/Ge (1500 Å)/Cu (1500 Å) multilayer metals are deposited on the GaAs wafer with Si-doped epitaxial layer (2000 Å, $1 x 10^{18}$ cm^{-3}). After annealing in a traditional tube furnace at different temperatures for 20 min, the results of the contact resistivities of the Pd(150 Å)/Ge(1500 Å)/Cu(1500 Å) ohmic contact extracted from the transmission line measurements (TLM) as a function of annealing temperature are shown in Figure 14. Low ohmic contact resisitivity can be obtained when the Pd/Ge/Cu ohmic samples were annealed at 220°C ~ 350°C for 20 min. The lowest specific contact resistivity was 5.73 x 10^{-7} Ω-cm^2 after the sample was annealed at 250 °C for 20 min.

In this study, the effect of the ohmic metal composition on the contact resistance is investigated. Figure 15 shows the ohmic characteristics of the Pd/Ge/Cu samples with different Pd thicknesses, the values of the lowest specific contact resistivity for these samples are listed in Table 4. As these

results indicate, the Pd/Ge/Cu sample with 150 Å Pd layer has the lowest specific contact resistivity and the thickness of Pd layer has a significant effect on the ohmic contact resistance. One may notice that the lowest specific contact resistivity of the Pd/Ge/Cu sample with 50 Å Pd appeared at 200 °C, it may be due to the formation of thinner Pd_xGaAs compound layer which made the Ge atoms diffuse through the thinner Pd_xGaAs compound layer into GaAs substrate easily. However, the adhesion between the 50 Å Pd layer and the GaAs surface was very weak, the ohmic metal peeled off easily.

Figure 16 shows the ohmic characteristics of the Pd/Ge/Cu samples with different Ge thicknesses, the values of the lowest specific contact resistivity for these samples are listed in Table 5. As these results indicate, the thickness of Pd layer has also a significant effect on the ohmic contact resistance. The Pd/Ge/Cu sample with 1500 Å and 2000 Å Ge layer have similar low specific contact resistivity, but the Pd/Ge/Cu ohmic contact with 1000 Å Ge layer has no ohmic characteristic. It may be due to that for the thinner Ge layer, there were not enough Ge atoms to react with Cu and diffuse into GaAs surface.

4.2 Formation Mechanism of The Pd/Ge/Cu Ohmic Contact

In this section, the formation mechanism of the Pd/Ge/Cu ohmic contact was investigated by results of XRD, SMIS, AFM, TEM and EDX. Use TEM image and EDX analysis for microstructure observation, X-ray diffraction for phase identification, AFM for surface morphology observation, and SIMS for interfacial elements material analysis. The results are shown below.

4.2.1 TEM and EDX for Microstructure Observation

Figure 17 shows the SEM image of the as-deposited Pd (150 Å)/Ge (1500 Å)/Cu (1500 Å) structure deposited on GaAs substrate. From this figure, the Pd, Ge, and Cu layers can be seen obviously. The thin Pd layer enhances the adhesion of the ohmic metal and the Cr layer was used as the anti-oxidation layer for Cu.

Figure 18 ~ Figure 22 shows the TEM images and EDX profiles of Pd/Ge/Cu ohmic metal structure after annealing at 150°C, 250°C, 400°C for 20min respectively. Figure 18(a) shows the TEM image of the sample after annealing at 150°C for 20 min. From this figure, a small proportion of Ge and Cu started to react with each other as the Pd/Ge/Cu ohmic metal structure annealing was annealed at 150°C for 20 min. However, from the EDX analysis, the Cu_3Ge grains were not formed and the Pd layer had no obvious reaction with Ge/Cu and GaAs substrate after 150°C annealing as shown in Figure 18(b). There was no ohmic behavior in Pd/Ge/Cu ohmic system after 150°C annealing.

The TEM image of the Pd/Ge/Cu ohmic metal structure after annealing at 250°C for 20 min is shown in Figure 19(a). From the figure, the Cu/Ge compound started to form grains with vertical grain boundary and long range order. From the EDX analysis, the grains were Cu_3Ge compound as shown in Figure 19(b). Literature shows that the compound has low metallic resistivity and Ga has lower chemical potential in Cu_3Ge than in GaAs compound [28]. On the other hand, Figure 20 shows the HRTEM image of the near-interface region between GaAs substrate and ohmic compound after 250°C annealing. The Pd_xGaAs phases started to appear at the GaAs surface after 250°C annealing. Due to Pd_xGaAs compound, it may create more Ga vacancies. The Ge atoms could easily diffuse into the Ga vacancies in the vicinity of the GaAs surface,

resulting in a heavy doping n^+-GaAs layer. So the ohmic contact characteristic of the Pd/Ge/Cu appeared after annealing at 250°C for 20 min.

The EDX profiles in Figure 21 show that there is still no Cu atom diffusing into GaAs the substrate near the Pd/GaAs interface after 250 ℃ annealing.

However, after annealing at 400°C for 20 min, obvious atomic inter-diffusion and interfacial reactions started to occur as can be seen from Figure 22. The ohmic contact characteristics of the Pd/Ge/Cu ohmic system started to degrade after 400°C annealing, the possible reasons for ohmic contact degradation were As atoms diffusing out and Ga atoms diffusing into the Ge layer. (Ga atoms acted as acceptors which reduced the donor concentration.)

4.2.2 X-ray Diffraction for Phase Identification

Figure 23 shows the x-ray diffraction profiles for the Pd (150 Å)/Ge (1500 Å)/Cu (1500 Å) ohmic contact structure as deposited and after annealing at 250 °C and 400 °C for 20 min. It can be seen from the XRD spectra that the diffraction peaks of Pd and Cu remained observable for the as deposited sample. It indicated that the Pd/Ge/Cu multi-layers did not react with each other for the as deposited sample. However, it is obvious from these data that the diffraction peaks of the Cu_3Ge compounds occurred and the diffraction peaks of Cu disappeared as the annealing temperature was higher than 250°C. The ohmic contact behavior was related to the formation of the Cu_3Ge compounds as the annealing temperature was above 250°C

4.2.3 SIMS for Interfacial Elements Material Analysis

Figure 24 shows the SIMS depth profiles after the sample was annealed at 250 °C for 20 min. From the SIMS profiles, it can be seen that the Ge atoms

diffused into GaAs and the Ga atoms diffused out into the ohmic layer. As mentioned above, both the formation of Cu_3Ge grains and Pd_xGaAs phases after annealing helped the inter-diffusion of the Ga and Ge atoms.

4.2.4 AFM for Surface Morphology Observation

Figure 25 shows the surface morphologies for the Pd/Ge/Cu ohmic metal system and the traditional Au/Ge/Ni ohmic system after annealing as measured by AFM. The root-mean-square (rms) roughness of the Pd/Ge/Cu sample is 4.541nm. The root-mean-square (rms) roughness of the traditional Au/Ge/Ni sample is 6.566nm. It is obviously that the surface morphology of Pd/Ge/Cu ohmic system is smoother than the traditional Au/Ge/Ni ohmic system.

4.3 Thermal Stability Test for The Pd/Ge/Cu Ohmic Contact

To study the thermal stability of the Pd (150 Å)/Ge (1500 Å)/Cu (1500 Å) ohmic contact, the Pd/Ge/Cu multilayer layer were annealed at 250°C for 24 hours and measured the specific contact resistivity was used TLM patterns. For comparison, the traditional Au/Ge/Ni ohmic system TLM patterns were also tested at the same conditions. Figure 26 shows the long time thermal stability test results. From this figure, it can be seen that there was no obvious degradation on the Pd/Ge/Cu ohmic system after annealing at 250 ℃ for 24 hours. The contact resistivity increased slightly after 250 ℃ annealing for 12 hours, and then kept at $8 \times 10^{-7}\ \Omega\text{-cm}^2$ for annealing time up to 24 hours. And the contact resistivity of Pd/Ge/Cu ohmic contact was still lower than that of traditional Au/Ge/Ni ohmic system after annealing at 250 ℃ for 24 hours. From the results shown above, it is clear that the Pd/Ge/Cu ohmic system to n-type

GaAs has low contact resistance and was quite stable even after long time annealing.

4.4 DC and RF Measurements

4.4.1 DC Measurements

Pd/Ge/Cu ohmic contact was applied to the fully Cu-metallized InGaP/GaAs HBTs as emitter and collector metal. In this fully Cu-metllized HBT, Pt/Ti/Pt/Cu was used as the base metal, SiN_x was used for passivation, and Ti/Pt/Cu for interconnect metal with Pt as the diffusion barrier. InGaP/GaAs HBTs with traditional n-type metal (Au/Ge/Ni/Au), and p-type metal (Pt/Ti/Pt/Au) contacts, and interconnect metal (Ti/Au) were also processed on half of the same wafer for performance comparison.

Figure 27 shows the optical microscope images of the fully Cu-metallized InGaP/GaAs HBTs with Pd/Ge/Cu ohmic contact after fabrication. Figure 28 shows the typical common emitter characteristics of HBTs with emitter area of 4 x 20μm^2. In the figure, one group of curves belongs to the fully Cu-metallized HBTs and the other one belongs to the traditional Au-metallized HBTs. It can be seen from Figure 28 that these two devices show similar knee voltage and offset voltage. We did not observe an increase in the knee voltage or the decay of the collector current, which indicates that the characteristics of the InGaP/GaAs HBTs with Pd/Ge/Cu ohmic contact are reasonably good. The common emitter current gain is around 130 for both cases. Gummel plots of the HBTs with the traditional Au HBT and Au free fully Cu HBT were also compared. The results are shown in Figure 29. The two HBTs also showed similar behavior.

To test the reliability of the Pd/Ge/Cu as the n-type ohmic metal for the

Cu-metallized HBTs, both copper and gold metallized HBTs with 4x20μm^2 emitter area were subjected to current accelerated stress test with high current density of 110 kA/cm^2. It is much higher than 25kA/cm^2 required for the normal device operation and the purpose is to shorten the stress time so that the stress tests could be performed at wafer level without using any package and the results could be obtained in a few hours [27]. Figure 30 plots the current gain (β) of the fully Cu-metallized HBTs with Pd/Ge/Cu ohmic contact after stressed at the high current density of 110 kA/cm^2 with V_{CE} of 2.5V for a period of 24 hours. The measurements were made at an amibient room temperature of T_A = 25°C. It can be seen from the data that the current gain of the device showed no significant change with time. The change in the ratio of the final/initial current gain was less than 4% for the device and was still higher than 115 after 24h of the current-accelerated stress test.

To study the thermal stability of the fully Cu-metallized HBT with Pd/Ge/Cu ohmic contact, the 4 x 20-μm-emitter-area HBT device was annealed at 250°C for 24 hours and tested for electrical performance. Figure 31 shows the common emitter I-V curves of the fully Cu-metallized HBT before and after annealing which shows no change in the offset voltage, knee voltage, and saturation current. Figure 32 shows the current gain (β) as a function of aging time at 250℃ for the 4x20-μm^2-emitter-area fully Cu-metallized HBT with Pd/Ge/Cu ohmic contact. It suggested that there was no ohmic degradation, copper oxidation, and copper diffusion in the fully Cu-metallized HBT with Pd/Ge/Cu ohmic contact after the annealing.

4.4.2 RF Measurements

The microwave performance of the fully Cu-metallized HBT with Pd/Ge/Cu ohmic contact was characterized by on-wafer S parameter measurement using a network analyzer. The h_{21} as a function of frequency were measured under collector-emitter voltage (V_{CE}) of 2V, 2.5V, and 3V. The base current was 0.06, 0.08, 0.1, 0.12, 0.14mA. The f_T was extrapolated with -20 dB/decade slope. Figure 33 shows the h_{21} curve at the V_{CE} = 2.5V and I_B = 0.14mA as a function of frequency. The cutoff frequency was about 38GHz. It is clear that the microwave performance of the fully Cu-metallized HBT with Pd/Ge/Cu ohmic contact is very good.

Tables

Table 4 The lowest specific contact resistivities of Pd/GeCu ohmic contact on n-type GaAs with different Pd thicknesses.

	Metal composition (Thickness Å)			**The lowest specific contact resistivity (Ω-cm^2)**
	Pd	**Ge**	**Cu**	
Sample 1	**0**	1500	1500	$\sim 10^{-5}$
Sample 2	**50**	1500	1500	7.43×10^{-7}
Sample 3	**150**	1500	1500	5.72×10^{-7}
Sample 4	**300**	1500	1500	7.88×10^{-7}

Table 5 The lowest specific contact resistivities of Pd/Ge/Cu ohmic contact on n-type GaAs with different Ge thicknesses.

	Metal composition (Thickness Å)			**The lowest specific contact resistivity (Ω-cm^2)**
	Pd	**Ge**	**Cu**	
Sample 1	150	**1000**	1500	No ohmic
Sample 2	150	**1500**	1500	5.72×10^{-7}
Sample 3	150	**2000**	1500	5.34×10^{-7}

Figures

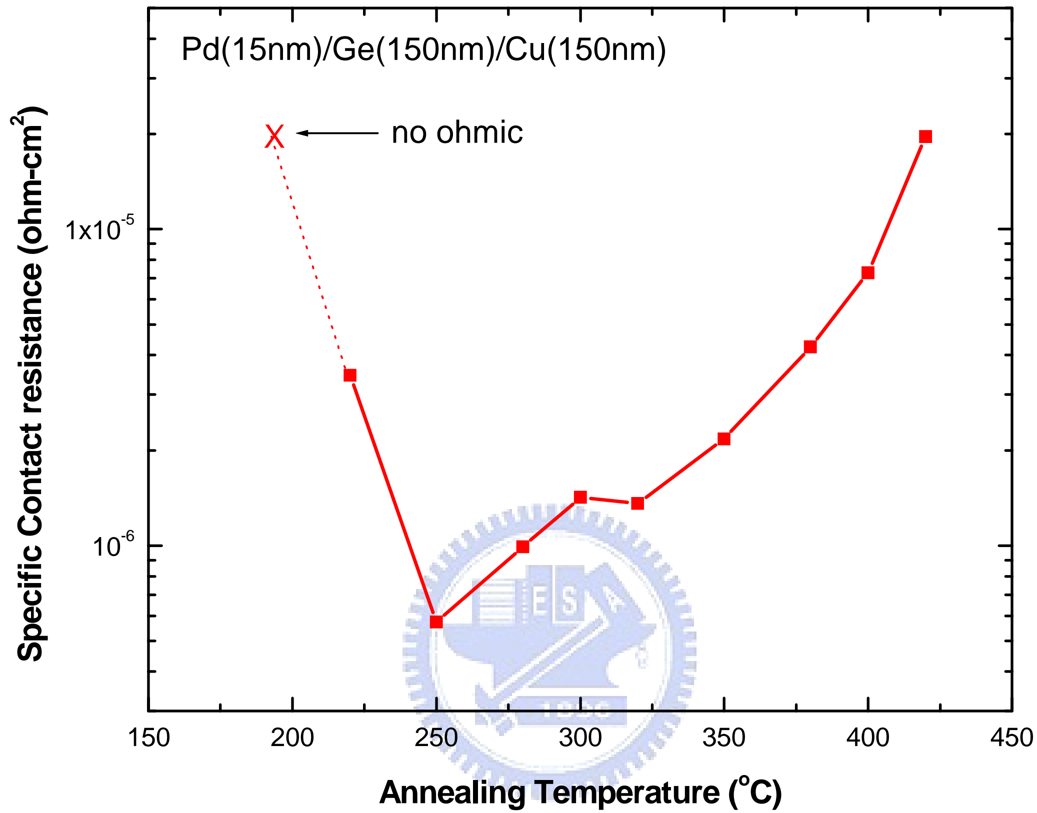

Figure 14 The specific contact resistivity of the Pd(15nm) / Ge(150nm) / Cu(150nm) contact on n-type GaAs as a function of annealing temperature.

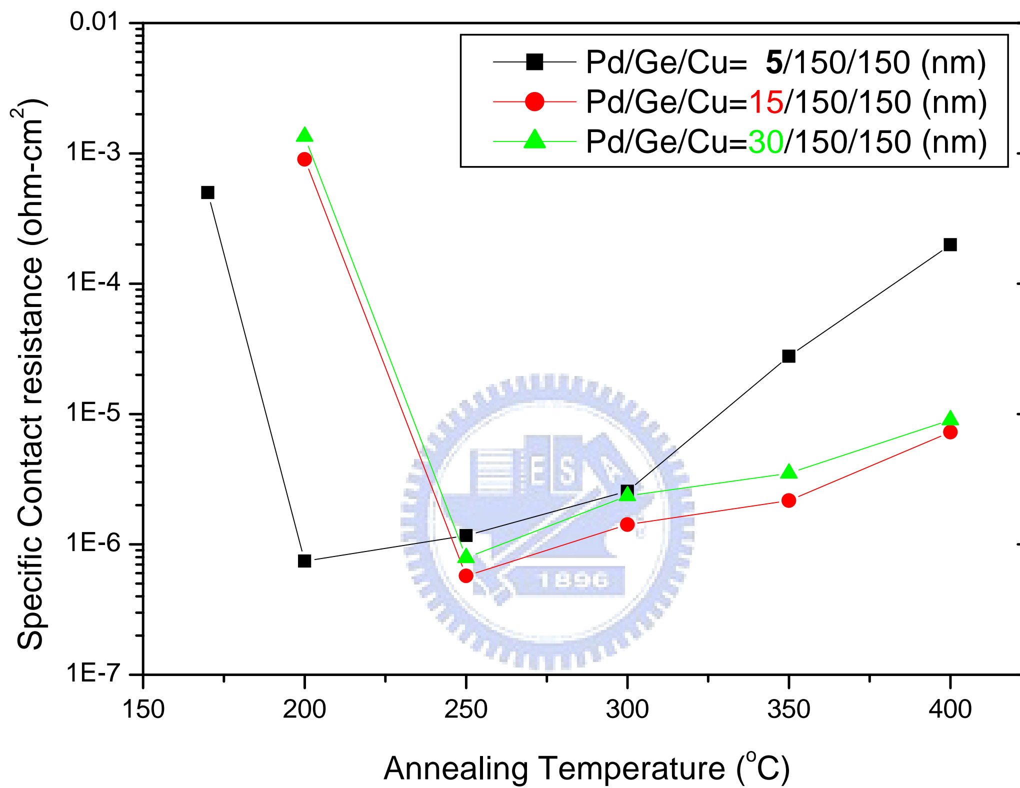

Figure 15 The specific contact resistivity as a function of annealing temperature of Pd/Ge/Cu ohmic contact on n-type GaAs with different Pd thicknesses.

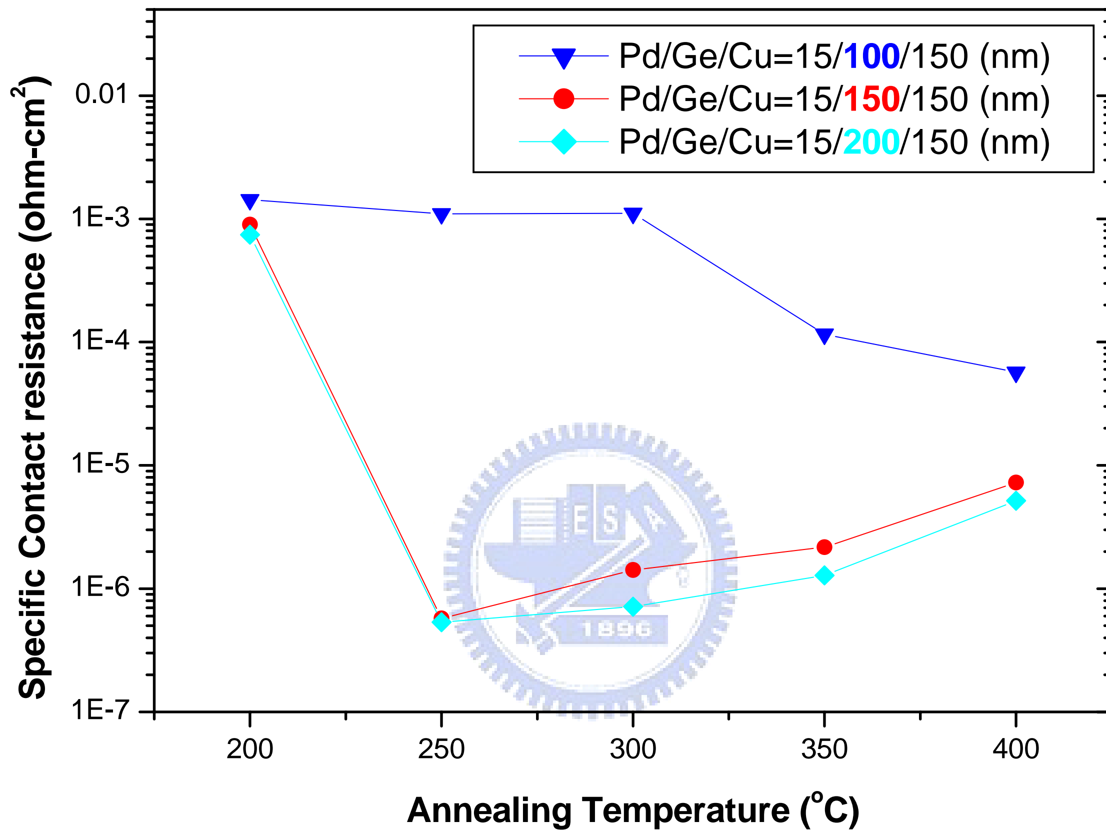

Figure 16 The specific contact resistivities as a function of annealing temperature of Pd/Ge/Cu ohmic contact on n-type GaAs with different Ge thickness.

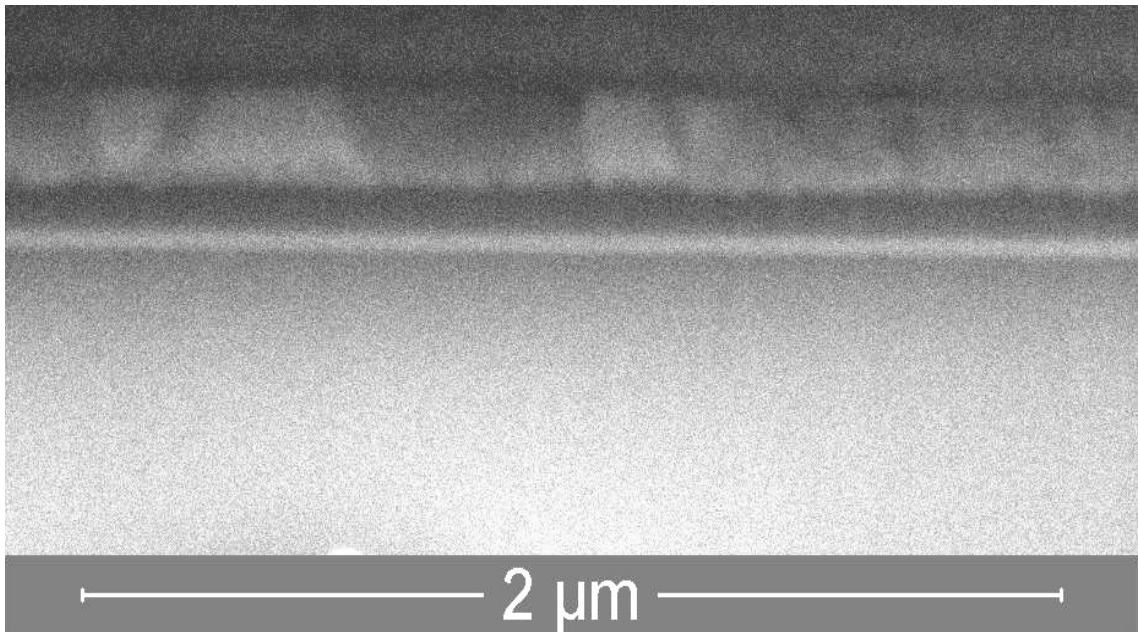

Figure 17 The SEM image of the Pd(15nm) / Ge(150nm) / Cu(150nm) contact for the as-deposited sample.

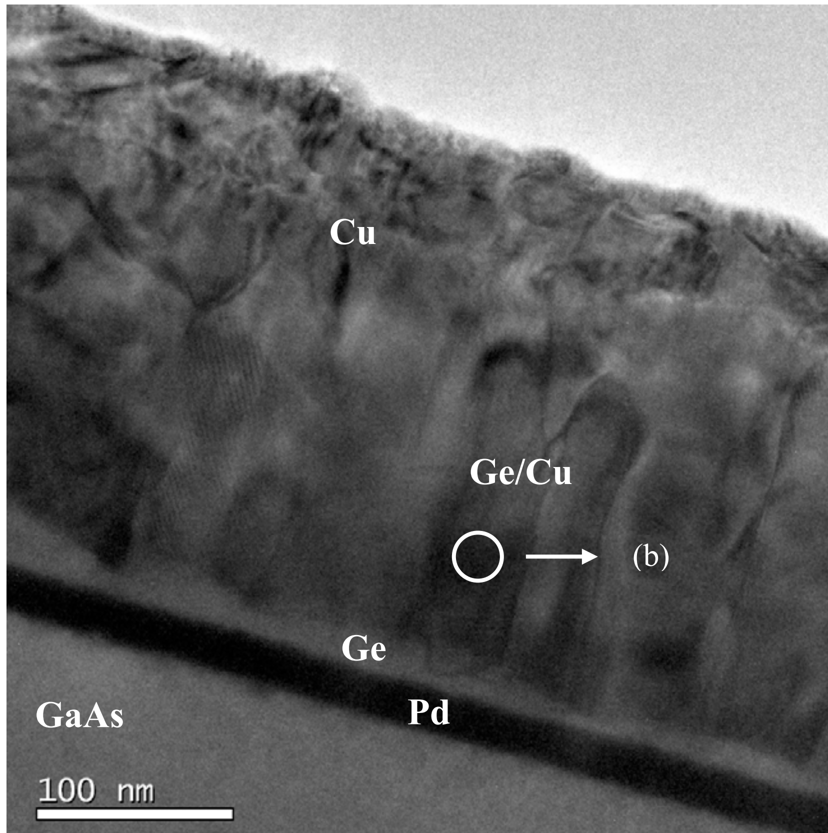

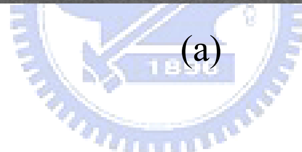
1896

(a)

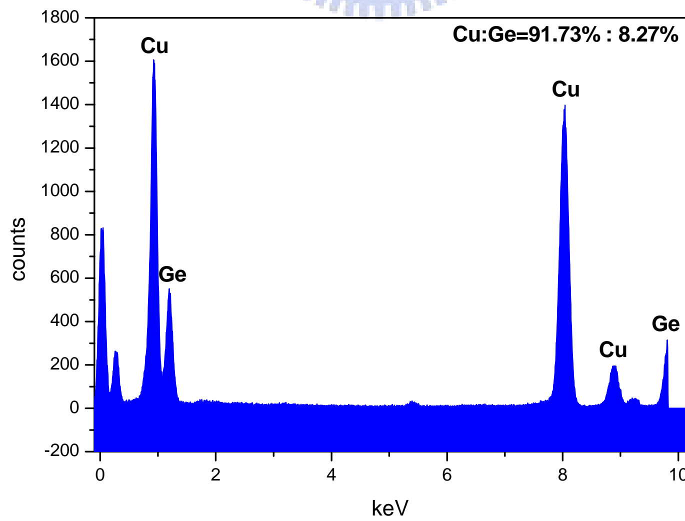

(b)

Figure 18 (a) The TEM image of the Pd/Ge/Cu contact cross section, (b) The EDX profiles of the Ge/Cu compound grains after annealing at 150℃ for 20 min.

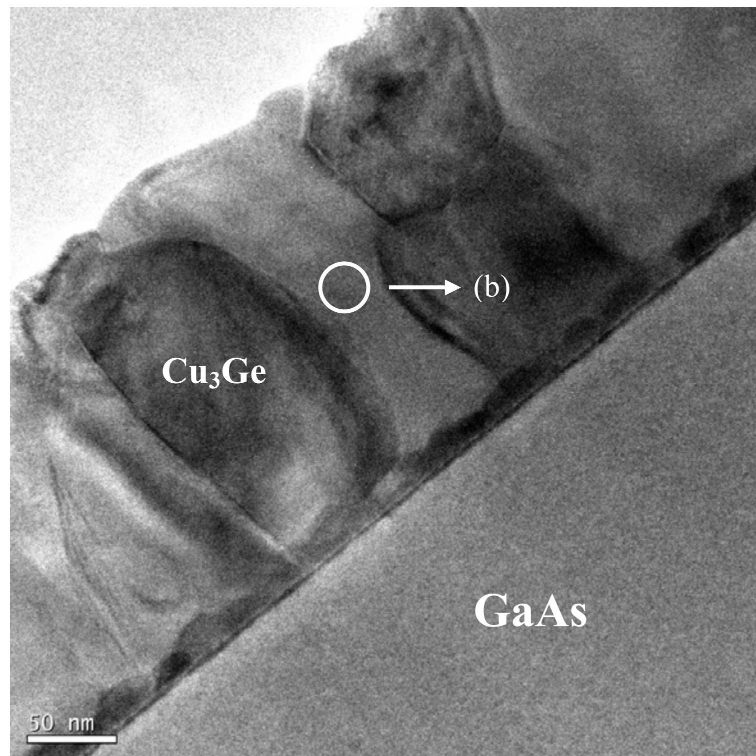

(a)

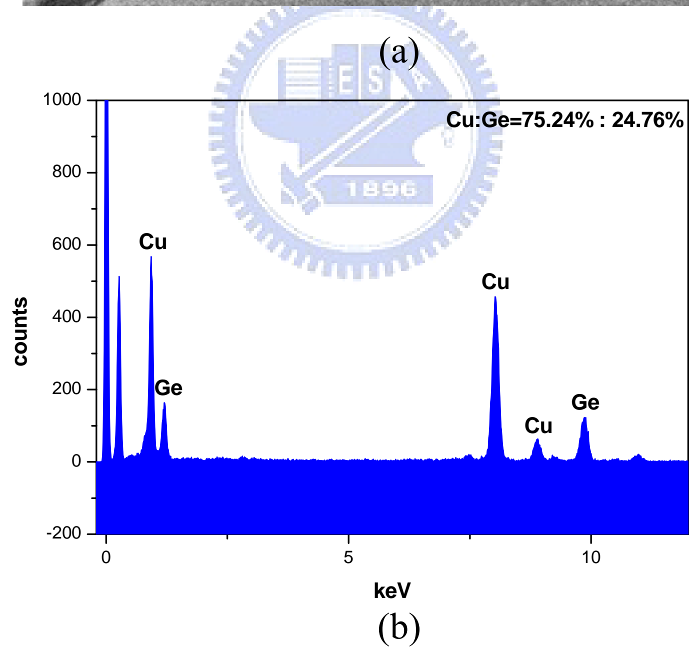

(b)

Figure 19 (a) The TEM image of the cross section of the Pd/Ge/Cu contact, (b) The EDX profile of the Cu_3Ge compound grains after annealing at 250℃ for 20 min.

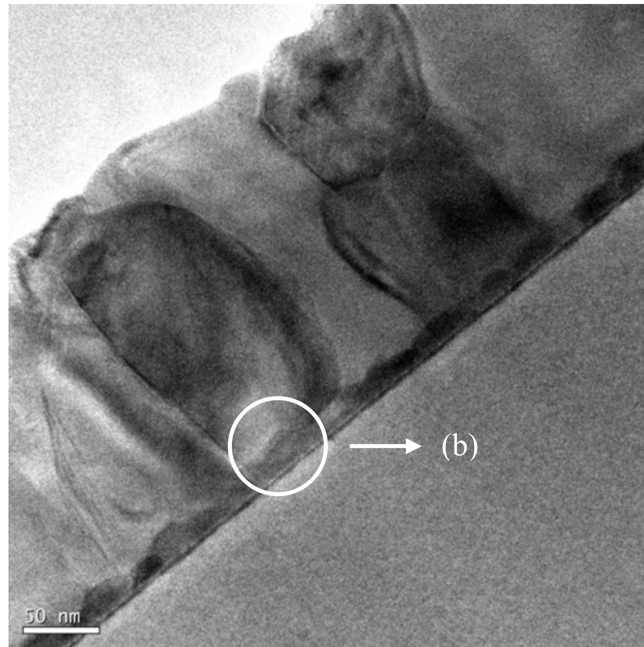

(a)

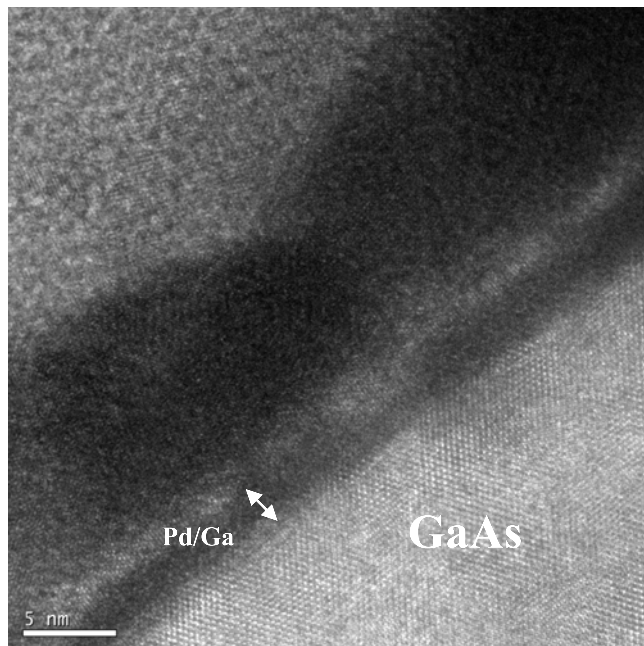

(b)

Figure 20 (a) The TEM image of the cross section of Pd/Ge/Cu contact, (b) The high resolution TEM image of the interface between the metallic compound in the ohmic metal layer and the GaAs substrate after annealing at 250℃ for 20 min.

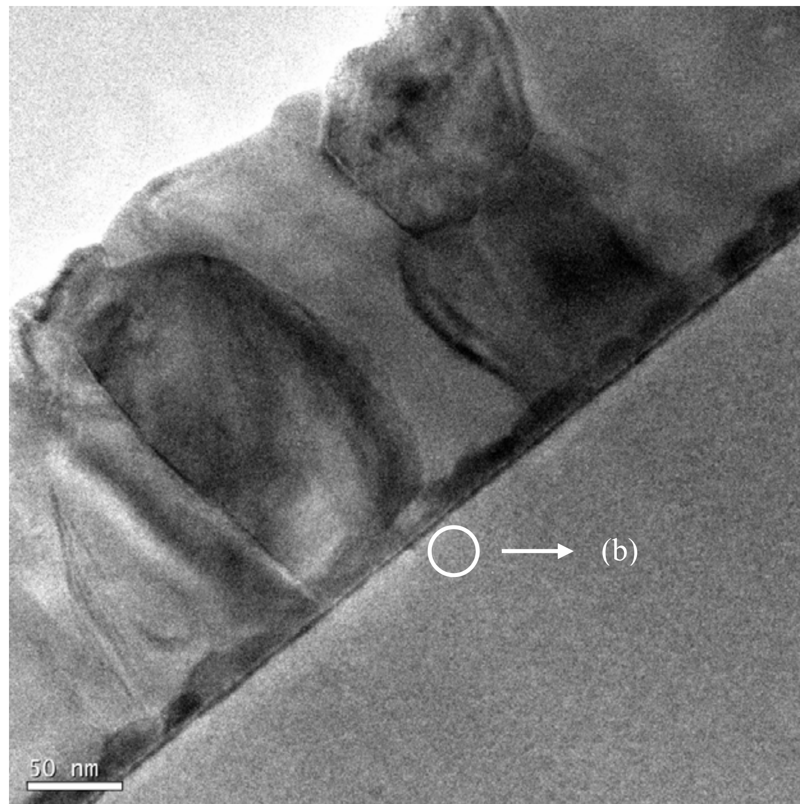

(a)

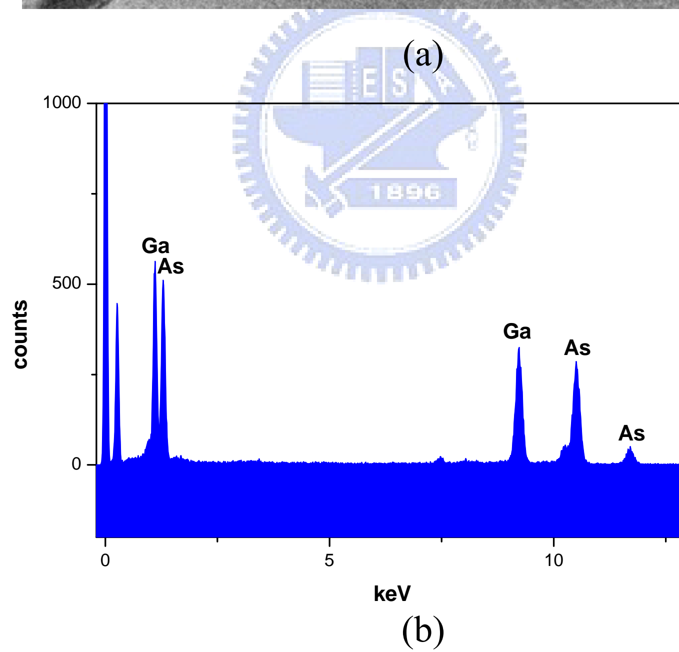

(b)

Figure 21 (a) The TEM image of the cross section of Pd/Ge/Cu contact, (b) The EDX profile of the near-interface region of the GaAs substrate after annealing at 250℃ for 20 min.

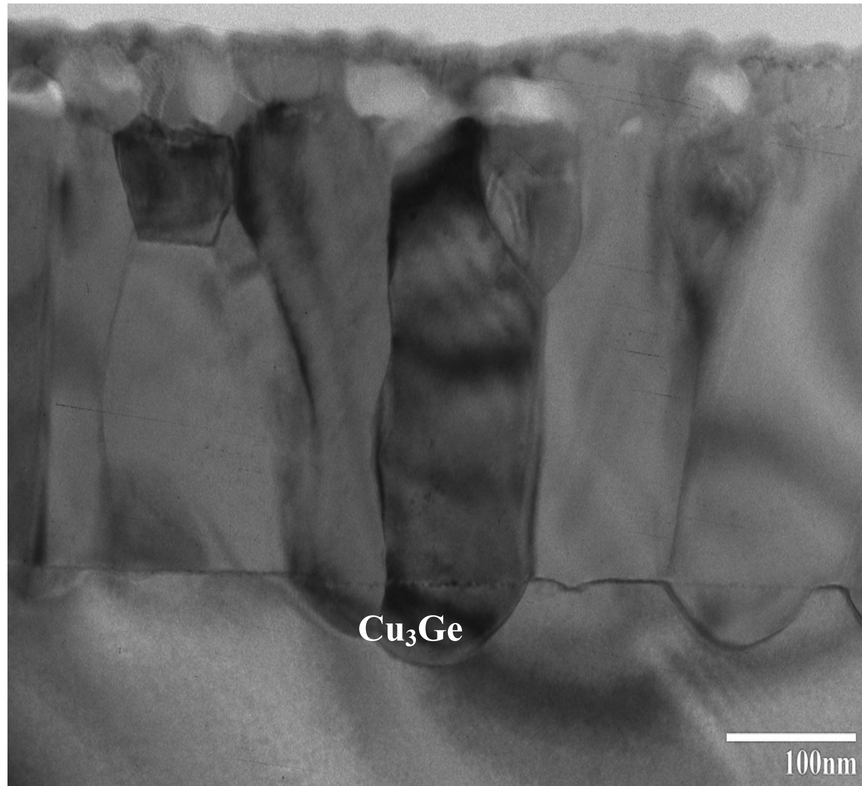

Figure 22 The TEM image of the cross section of the Pd/Ge/Cu contact after annealing at 400℃ for 20 min.

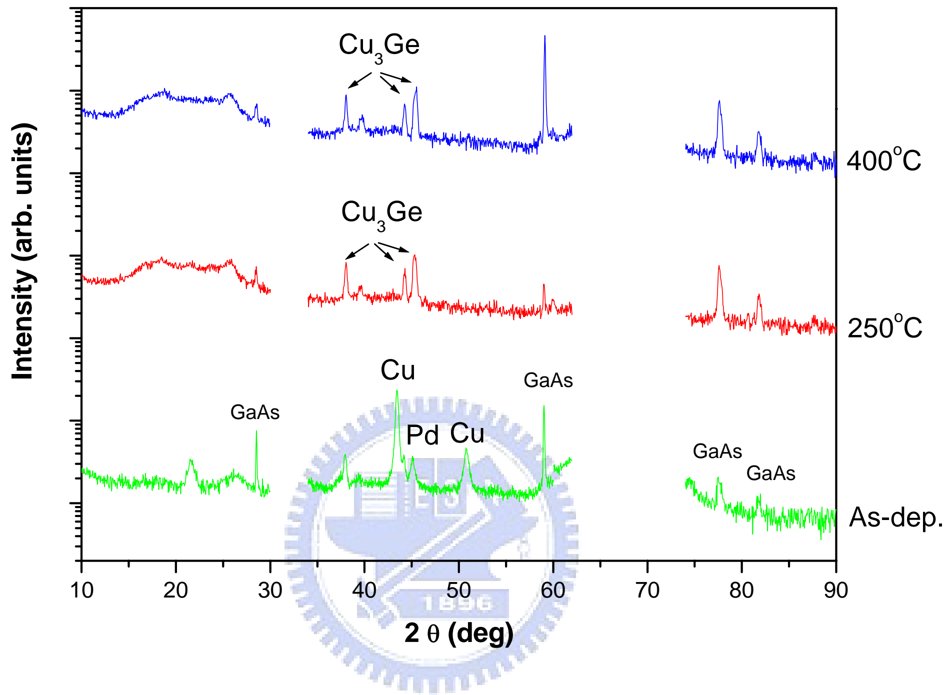

Figure 23 The X-ray diffraction patterns for the Pd (150 Å)/Ge (1500 Å)/Cu (1500 Å) contact after annealing at 250 °C for 20min, 400 °C for 20min, and the as-deposited sample.

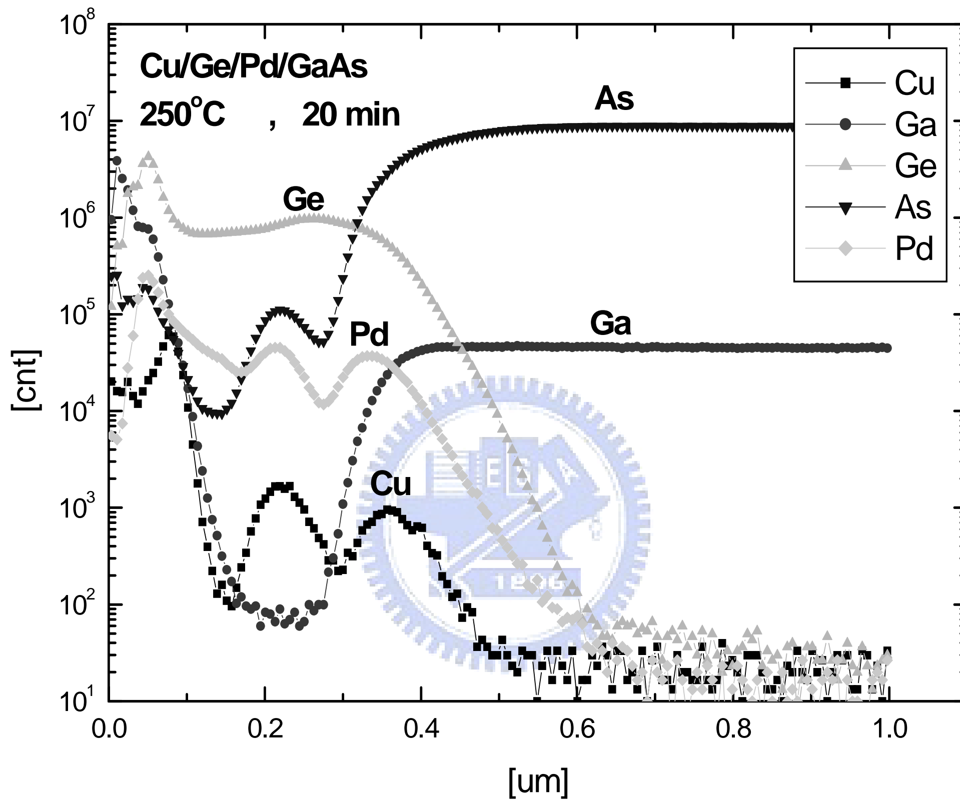

Figure 24 SIMS profiles of the Pd (150 Å)/Ge (1500 Å)/Cu (1500 Å) contact after annealing at 250 °C for 20min.

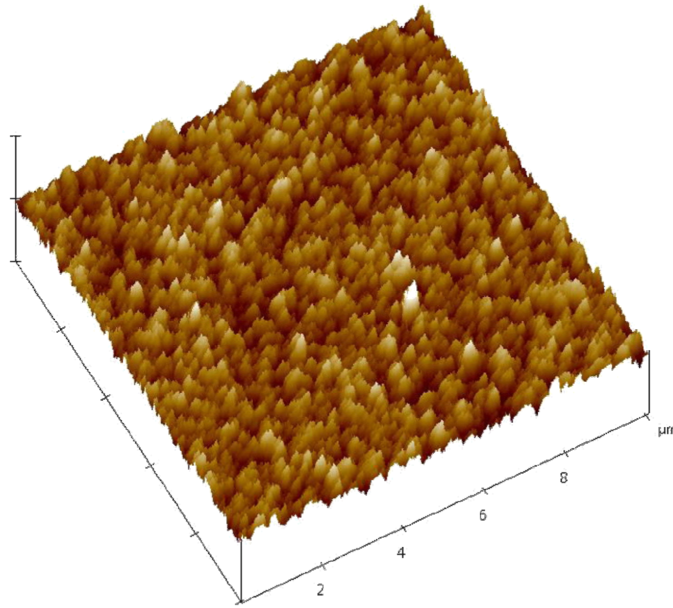

(a)

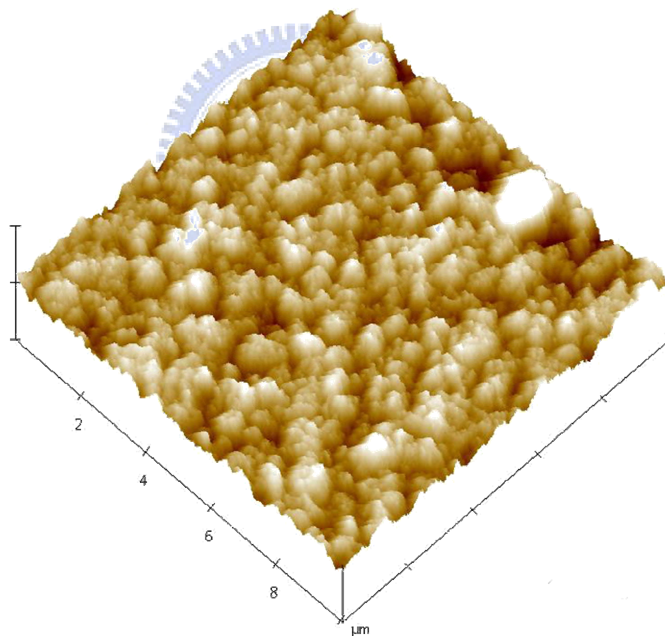

(b)

Figure 25 The AFM images of (a) the Pd/Ge/Cu ohmic contact after annealing at 250℃ for 20 min, (b) the Au/Ge/Ni/Au ohmic contact after RTA at 380℃ for 30 sec.

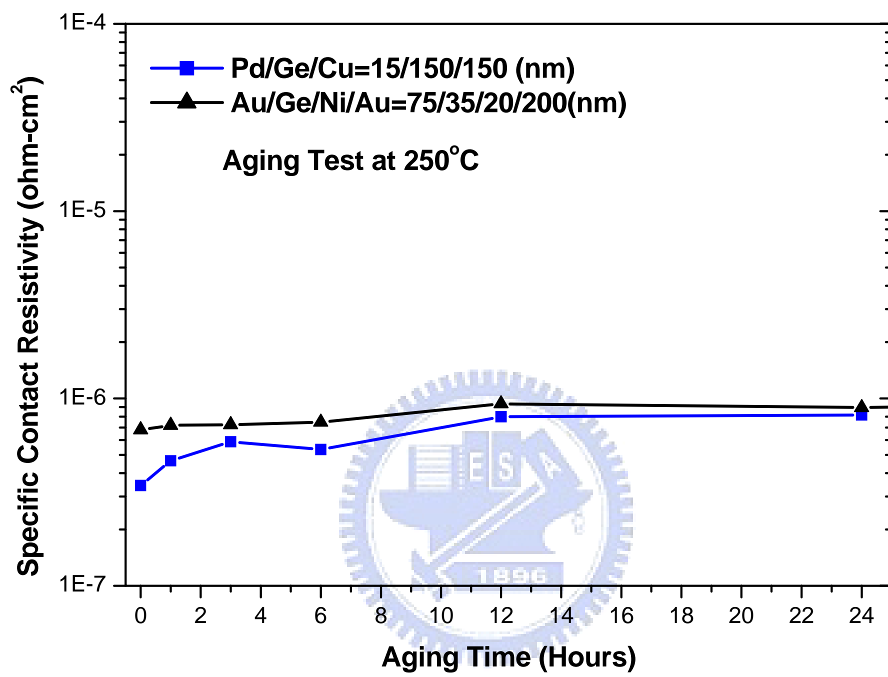

Figure 26 The specific contact resistivities of the Pd/ Ge/ Cu ohmic contact and Au/Ge/Ni/Au ohmic contact on n-type GaAs as a function of aging time.

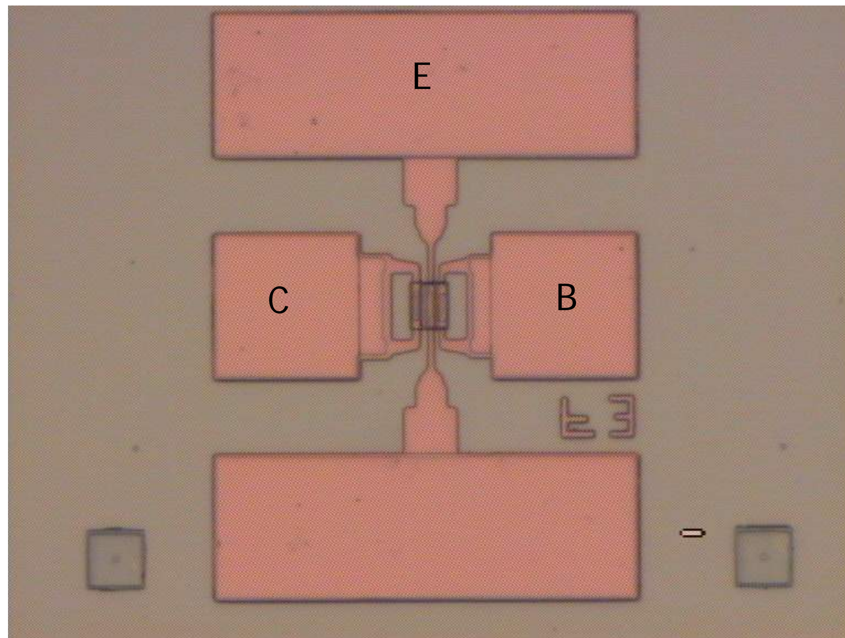

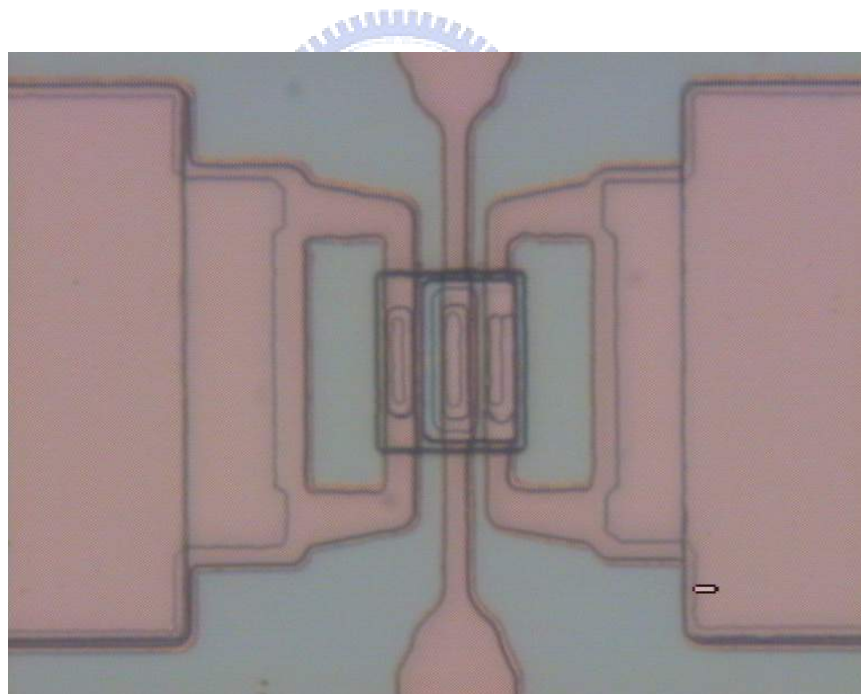

Figure 27 The OM images of Au-free fully-Cu InGaP/GaAs HBT with Pd/Ge/Cu as n-type ohmic contact device.

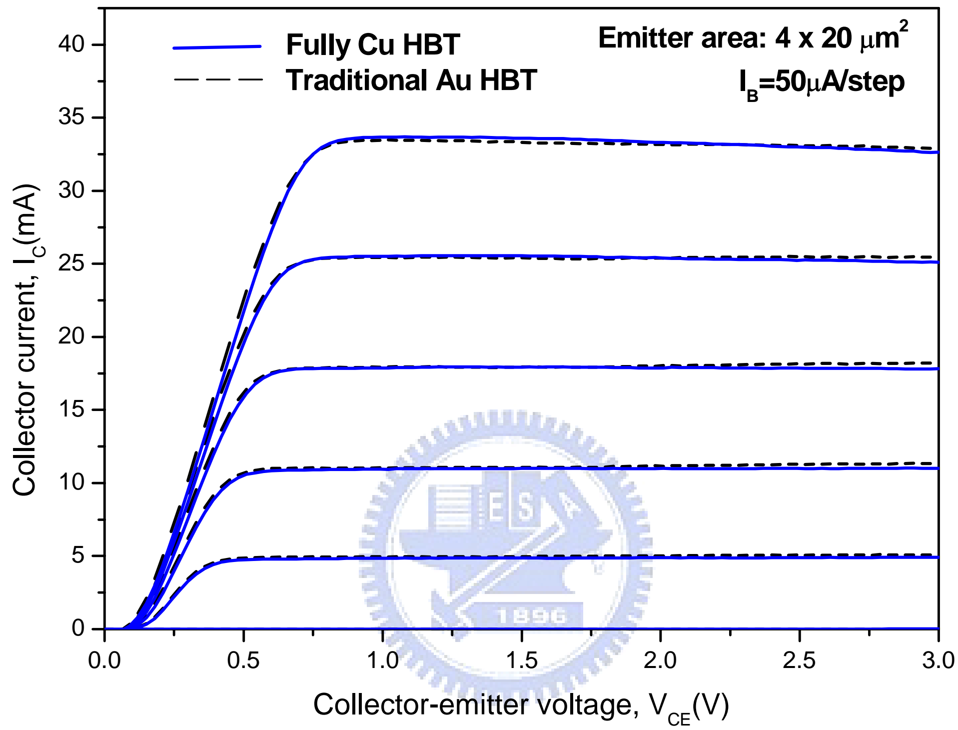

Figure 28 Comparison of the typical I_C-V_{CE} characteristics for the emitter area(4 x 20 μm^2) HBTs with Cu and with Au metallizations.

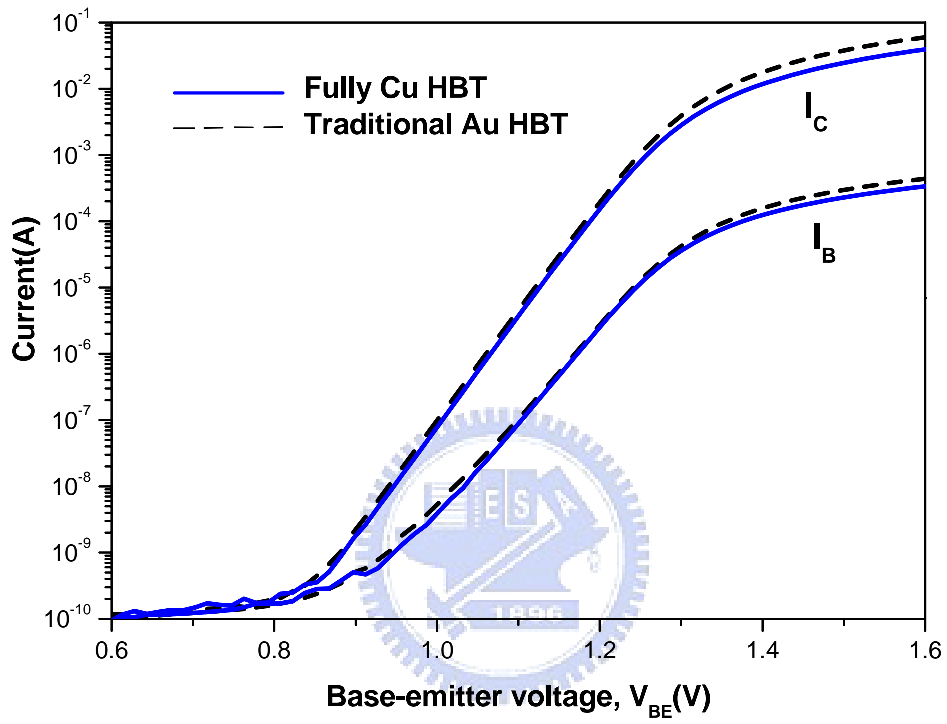

Figure 29 Comparison of Gummel plots for the emitter area(4 x 20 μ m^2) HBTs with Cu and with Au metallizations.

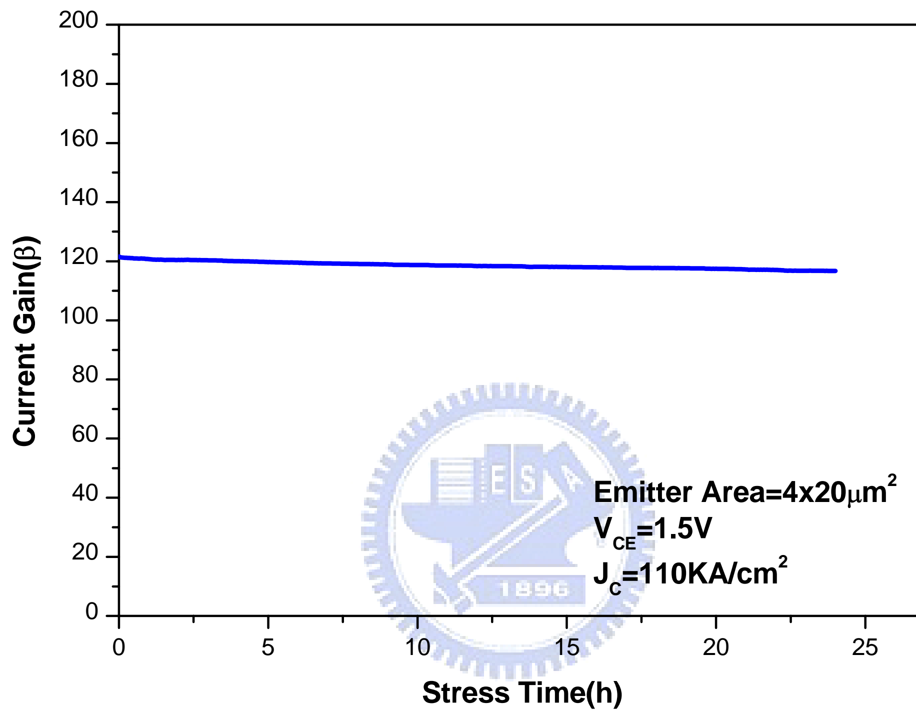

Figure 30 The current gain (β) as a function of stress time at constant I_B for the 4x20- μ m^2-emitter-area fully Cu-metallized HBT with Pd/Ge/Cu ohmic contact.

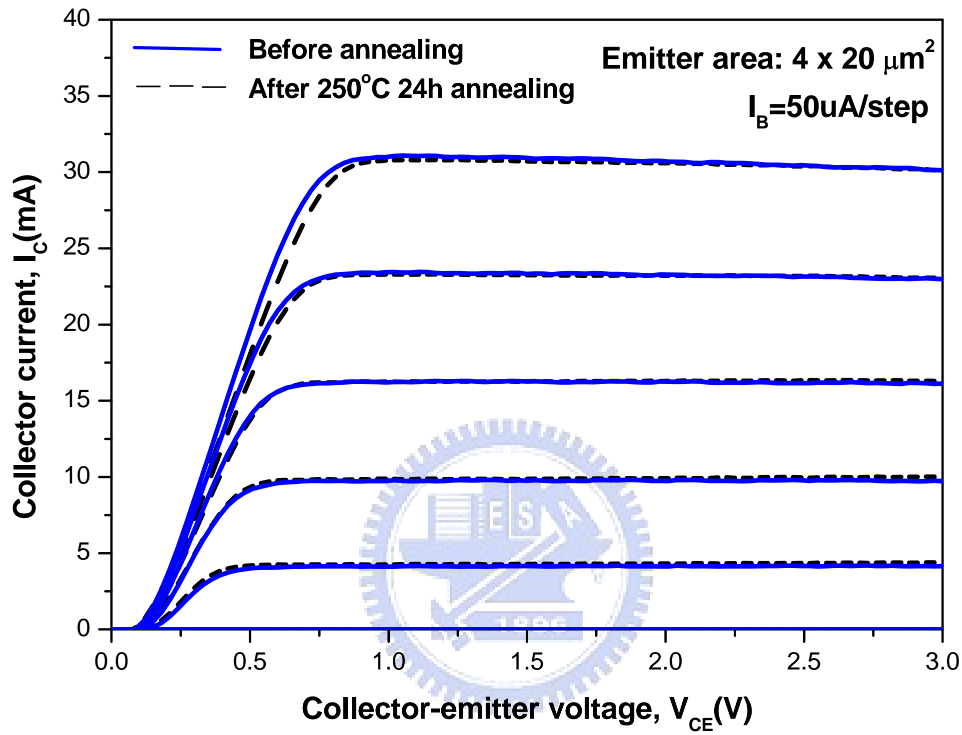

Figure 31 Common emitter I-V curves measured before and after annealing at 250℃ for 24 h for the 4x20-μm^2-emitter-area fully Cu-metallized HBT with Pd/Ge/Cu ohmic contact.

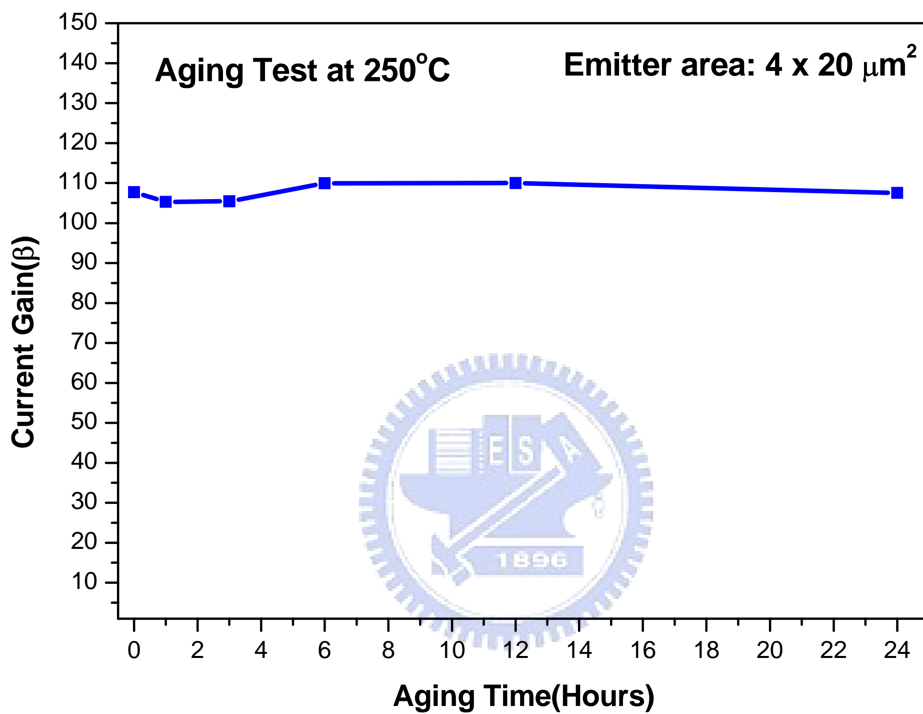

Figure 32 The current gain (β) as a function of aging time at 250℃ for the 4x20- μm^2-emitter-area fully Cu-metallized HBT with Pd/Ge/Cu ohmic contact.

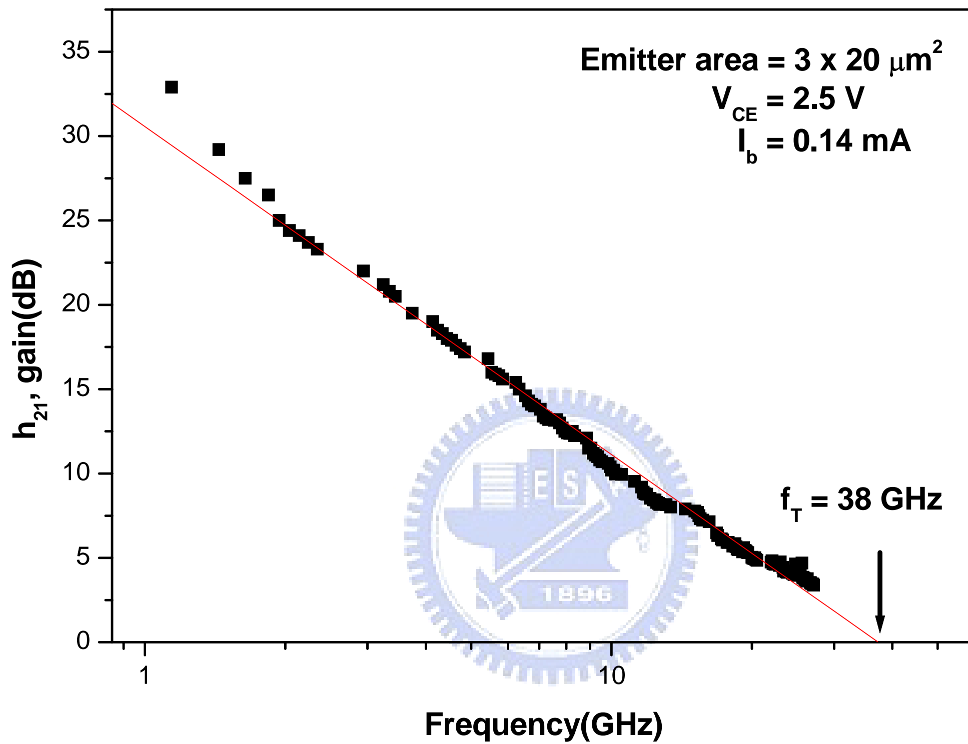

Figure 33 Current gain H_{21} curves measured for the 3x20- μ m emitter-area fully Cu-metallized HBT.

Chapter 5
Conclusions

In this study, a novel Pd/Ge/Cu ohmic contact to n-type GaAs has been successfully developed. The Au-free fully Cu-metallized InGaP/GaAs HBTs using Pd/Ge/Cu ohmic contact to n-type GaAs also has been successfully fabricated for the first time.

The optimized Pd (150 Å)/Ge (1500 Å)/Cu (1500 Å) metal structure forms a low contact resistivity ohmic contact to n-type GaAs at a low annealing temperature. Low ohmic contact resistivity can be obtained when the Pd/Ge/Cu ohmic samples were annealed at 220°C ~ 350°C for 20min. The lowest specific contact resistivity achieved was 5.73×10^{-7} Ω-cm^2 when annealed at 250 °C for 20 min. The thicknesses of the Pd and Ge layers play an important role on the ohmic contact resistivity. The thin Pd layer enhances the adhesion of the ohmic metals and helps the Ge atoms (donor) diffuse into the Ga vacancies. The enough thickness of Ge layer enhances good ohmic contact characteristic.

From SIMS, XRD, TEM, and EDX studies, the low contact resistivity was due to the formation of the Cu_3Ge compound and the Pd_xGaAs compound in conjunction with the outdiffusion of Ga into the ohmic metal and the diffusion of Ge into the Ga vacancies. From AFM results, the surface morphology of Pd/Ge/Cu ohmic contact was smoother than the traditional Au/Ge/Ni ohmic contact. The contact resistivity of Pd/Ge/Cu ohmic contact was also very stable after annealing at 250°C for 24 hours. And the contact resistivity of Pd/Ge/Cu ohmic contact was still lower than that of traditional Au/Ge/Ni ohmic system after 24 hours annealing. Overall, the Pd/Ge/Cu ohmic contact has a low contact

resistivity, good thermal stability, and good surface morphology.

The Pd/Ge/Cu ohmic contact was applied to fully Cu-metallized InGaP/GaAs HBTs. In this fully Cu-metallized HBT, Pt/Ti/Pt/Cu was used as the base metal, SiNx was used for passivation, and Ti/Pt/Cu was used for interconnect metals with Pt as the diffusion barrier. The common emitter I-V curves and Gummel plot of these Cu-metallized HBT using Pd/Ge/Cu ohmic contact showed similar electrical characteristics as those for HBT metallized with conventional Au-metallized HBT. The common emitter current gain for the 4x20-μm^2-emitter-area of fully Cu-metallized HBT using Pd/Ge/Cu ohmic contact and traditional Au-metallized HBT were both around 130. The cutoff frequency (f_T) of 3x20-μm^2-emitter-area devices was about 38GHz at V_{CE} = 2.5V and I_b = 0.14mA. It is clear that the microwave performance of the fully Cu-metallized HBT with Pd/Ge/Cu ohmic contact is very good.

During both the current-accelerated stress test (110 kA/cm^2 stress for 24h) and the thermal stability test (annealing at 250°C for 24 hours), for the fully Cu-metallized HBT with Pd/Ge/Cu ohmic contact showed almost no obvious degradation in electrical characteristics. The results show that the novel Pd/Ge/Cu ohmic contact can be used on Au-free fully Cu-metallized InGaP/GaAs HBTs, and exhibits good device performance.

Reference

[1] K. Holloway and P. M. Fryer, “Tantalum as a diffusion barrier between copper and silicon,” *Appl. Phys. Lett.*, vol. 57, no. 17, pp. 1736-1738, Oct. 22, 1990.

[2] K. Holloway, P. M. Fryer, C. Cabral, Jr., J. M. E. Harper, P. J. Bailey, and K. H. Kelleher, “Tantalum as a diffusion barrier between copper and silicon: failure mechanism and effect of nitrogen additions,” *J. Appl. Phys.*, vol. 71, no. 11, pp. 5433-5444, 1992.

[3] D. S. Yoon, H. K. Baik, and S. M. Lee, “Effect on thermal stability of a Cu/Ta/Si heterostructure of the incorporation of cerium oxide into the Ta barrier,” *J. Appl. Phys.*, vol. 83, no. 12, pp. 8074-8076, 1998.

[4] C. Y. Chen, L. Chang, E. Y. Chang, S. H. Chen, and D. F. Chang, “Thermal stability of Cu/Ta/GaAs multilayers,” *Appl. Phys. Lett.*, vol. 77, no. 21, pp. 3367-3369, 2000.

[5] C. Y. Chen, E. Y Chang, L. Chang, and S. H. Chen, “Backside copper metallisation of GaAs MESFETs,” *Electronics Lett.*, vol. 36, no. 15, pp. 1318-1319, 2000.

[6] C. Y. Chen, E. Y. Chang, L. Chang, and S. H. Chen, “Backside copper metallization of GaAs MESFETs using TaN as the diffusion barrier”, *IEEE Trans. Electron Devices*, vol. 48, no. 6, pp. 1033-1036, 2001.

[7] H. C. Chang, E. Y. Chang, Y. C. Lien, L. H. Chu, S. W. Chang, R. C. Huang and H. M. Lee, ” Use of WN_X as the diffusion barrier for copper airbridged low noise GaAs PHEMT”, *Electron. Lett,* Vol. 39, pp. 1763, 2003.

[8] S. W. Chang, E. Y. Chang, C. S. Lee, K. S. Chen, C. W. Tseng, T. L. Hsieh, "Use of WN_X as the Diffusion Barrier for Interconnect Copper Metallization of InGaP-GaAs HBTs", *IEEE TRANSACTIONS ON ELECTRON DEVICES*, VOL. 51, NO. 7, 2004.

[9] S. W. Chang, E. Y. Chang, "Gold-Free Fully Cu-Metallized InGaP/GaAs Heterojunction Bipolar Transistor", *Jpn. J. Appl. Phys.*, vol. 44, No. 1A, pp. 8-11, 2005.

[10] A. G. Baca and F. Ren, "A survey of ohmic contact to Ⅲ-Ⅴcompound semiconductors", *Thin solid films*, vol. 308, pp. 599-606, 1997.

[11] M. Murakami, "Development of refractory ohmic contact materials for gallium arsenide compound semiconductors," *S. and T. Advanced Materials*, Vol.3, pp1~27, 1-27, 2002.

[12] James W. Mayer and S. S. Lau, "Electronic Materials Science: For Intergrated Circuits in Si and GaAs" pp102

[13] T. lalinsky, On the technology, electrical characterization and reliability of ohmic contacts on GaAs, Elektrotech Cas. 37 pp.354-370, 1986.

[14] A. K. Niessen, model predictions for the enthalpy of formation of transition metal alloys, CALPHAD 7 pp. 51-70, 1983.

[15] W. Hume-Rothery, Inst. Metals pp.205, 1937.

[16] E. D. Marshell, Nonalloyed ohmic contact to n-GaAs by solid-phae epitaxy of Ge, *J. Appl. Phys*. 62, 1987.

[17] E. D. Marshall et al."Nonalloyed ohmic contacts to n-GaAs by soild-phase epitaxy of Ge," *J. Appl. Phys*, Vol.62, No.3, 1987.

[18] E. D. Marshall et al., "Nonalloyed ohmic contacts to n-GaAs by soild-phase epitaxy of Ge," *J. Appl. Phys*, Vol.62, No.3, 1987.

[19] M. S. Islam et al., ”Thermal stability of the non-alloyed Pd/Sn and Pd/Ge ohmic contacts to n-GaAs,”*Thin Solid Films*,Vol. 308-309, pp.607-610, 1997.

[20] W. D. Chen et al., ”Microstructure studies of PdGe/Ge ohmic contacts to n-type GaAs formed by rapid thermal annealing,”*Applied surface Science*, Vol. 100-101, pp.530-533, 1996.

[21] P. Machac et al., “Raman spectroscopy of Ge/Pd/GaAs contacts,” Microelectronic Engineering, Vol.71, pp177-181, 2004.

[22] M. O. Aboelfotoh et al., ‘Microstructure characterization of Cu_3Ge / n-type GaAs ohmic contacts,” J. Appl. Phys. Vol. 76, 1994.

[23] H. Kroemer, “Theory of a wide-gap emitter for transistors”, Proc. IRE 45, 1535, 1957.

[24] P. Asbeck et al., “Heterojunction bipolar transistors for microwave and millimeter-wave integrated circuits”, *IEEE Trans. Microwave Theory Tech. vil*, 1462, 1987.

[25] D. K. Schroder, Semiconductor Material and Device Characterization, Wiley-Interscience, Canada, 1998.

[26] W. C. Liu, J. H. Tsai, and S. L. Liu, *IEEE Electron Device Lett*. 13, 418, 1992.

[27] A. Gupta, A. Young and B. Bayraktaroglu, “InGaP makes HBT realibility a non-issue”, in GaAs Mantech Tech. Dig., 203, 2001.

[28] M. O. Aboelfotoh, C. L. Lin, and J. M. Woodall, “Novel low-resistance ohmic contact to n-type GaAs using Cu_3Ge”, *Appl. Phys. Lett.* 65 (25), 1994.